Independent University **Bangladesh (IUB)**

IUB Academic Repository

Dept. of Physical Science Article

2025-02

The LHCb Detector and Testing and Performance Evaluation of AdePT in Gaussino

Gomes, James Peter

IUB

http://ar.iub.edu.bd/handle/11348/1000

Downloaded from IUB Academic Repository



Independent University, Bangladesh (IUB)

Department of Physical Sciences

The LHCb Detector and Testing and Performance Evaluation of AdePT in Gaussino

PHY499: Project in Physics

Report submitted in partial fulfillment of the requirements

for the degree of BSc (Hons.) in Physics

James Peter Gomes

Student ID: 2022143

Under the supervision of Prof. M. Arshad Momen

27th February, 2025

Declaration

I, **James Peter Gomes**, declare that this thesis, titled **"The LHCb Detector and Testing and Performance Evaluation of AdePT in Gaussino"**, based on my project in the CERN Summer Student Program 2024, was completed as part of the **Senior Project Course** for my BSc (Hons.) in Physics Degree at **Independent University, Bangladesh** and that no other sources or learning aids, other than those listed, have been used. Furthermore, I declare that I have acknowledged the work of others by providing detailed references of the said work.

Signature of the student: _____

Certification of The Report

The report titled **"The LHCb Detector and Testing and Performance Evaluation of AdePT in Gaussino"**, submitted by James Peter Gomes, Student ID: 2022143, has been accepted as satisfactory in partial fulfillment of the requirements for the degree of BSc (Hons.) in Physics on **"27th February, 2025"**.

Members of the Assesment Committee:

Prof. M. Arshad Momen, PhD
(Supervisor): _____

Farhad Alam, PhD
(Head of the Department of
Physical Sciences): _____

Prof. Mohammad Mostofa Kamal, PhD
(Member): _____

Asma Begum, PhD
(Member): _____

Md. Readul Mahmud, PhD
(Member): _____

Jewel Kumar Ghosh, PhD
(Member): _____

Approval

The thesis titled

"The LHCb Detector and Testing and Performance Evaluation of AdePT in Gaussino"

submitted by **James Peter Gomes** has been examined and approved as a partial fulfilment of the requirements for the Senior Project Course at **Independent University, Bangladesh**.

Approved by:

Signature of Supervisor: _____

Signature of the
Head of the Department: _____

Signature of the
Director GSRIR: _____

Abstract

To meet the increasing computational demands of LHC experiments, this study explores the potential of GPU acceleration for electromagnetic simulations. The AdePT prototype is integrated into the Gaussino framework and compared to the standard GEANT4. Initial results show that AdePT, while requiring optimization, demonstrates promising performance gains, especially with larger workloads. The successful simulation of electrons using AdePT highlights its potential for accelerating LHCb simulations and contributing to future physics analysis. Furthermore, a brief review of the LHCb detector is provided, encompassing its key subdetectors: the Vertex Locator (VELO), the tracking system (including the Trigger Tracker, Inner Tracker, and Outer Tracker), the Ring Imaging Cherenkov (RICH) detectors, the electromagnetic and hadronic calorimeters (ECAL and HCAL), and the muon system.

Dedication

To my mother,

This thesis is dedicated to you.

This achievement is as much yours as it is mine. You shared in my struggles and sleepless nights. You have always trusted my decisions, never questioned my plans, and believed in my career goals. Giving you the life you have always wanted has become the purpose of my life.

You have been endlessly patient and have made countless sacrifices for me and everyone else. You deserve a much better life.

Ma, I know you're already very proud of me, but please be a little more patient and stay healthy because I want you to witness my success.

Acknowledgements

I express my deepest gratitude to everyone who has supported me throughout my academic journey and personal development.

First and foremost, I am profoundly grateful to my supervisor, Prof. M. Arshad Momen, for his invaluable guidance, insightful feedback, and unwavering encouragement at every stage of my academic journey. His patience and mentorship have not only shaped my academic growth but also taught me essential life lessons. A special thanks goes to him for teaching me the importance of "habit" in life and to contribute in keeping a stable mental health.

I am very thankful to my supervisors during the CERN Summer Student Program 2024, Witold Pokorski and Adam Morris for guiding me all the way during those eight weeks of the internship. They have been extremely friendly and welcomed me as an associated personnel to their simulation team very warmly. They have been very patient with my numerous questions, no matter how elementary they were at a machine perspective. I am also thankful to all the other researchers in the team who had been very prompt at replying to my queries even after office hours.

I am deeply indebted to my grandparents and maternal uncles for their endless love, understanding, and steadfast support. Their financial assistance and emotional encouragement have been instrumental in helping me reach where I am today.

I owe a special debt of gratitude to my senior, Md. Erfanul Haque Sajib, for standing by me during my toughest times. Even now, he checks in every other day just to see how I'm doing. His kindness and guidance have taught me invaluable lessons about what it truly means to be a good human being.

I would also like to extend my sincere thanks to my seniors, Irfan Sadat Ameen, Masruk Uddin, and Shafakat Arifeen, for the stimulating discussions, their insightful perspectives

on physics, and for fostering a positive and collaborative study environment.

Finally, I gratefully acknowledge the Department of Physical Sciences, along with every faculty member, staff, and fellow student, for being a second family to me. The memories we've created together will always hold a special place in my heart and will endure a lifetime.

Contents

1 Introduction **1**

1.1 Simulation in High Energy Physics 1

1.2 Monte Carlo Simulation 1

1.2.1 Event Generation 2

1.2.2 Detector Simulation and Particle Transport 4

1.3 GEANT4 4

1.4 Geometry Description Markup Language (GDML) 5

1.4.1 GDML Schema 6

1.4.2 GDML Reader and Writer 8

1.5 AdePT 9

1.6 Purpose of the Research 9

2 What is a Detector? **12**

2.1 Scintillation Counter 14

2.2 Multiwire Proportional Chamber 16

2.2.1 Time Projection Chamber (TPC) 17

2.3 LHC and Modern Detectors 19

2.3.1 How does the LHC operate? 19

2.3.2 General Purpose Detectors 21

3 CP Violation and LHCb **23**

3.1 Parity Violation 23

3.2 Charge Conjugation Violation and CP Symmetry 24

3.3 CP Violation 25

3.4 Objectives of the LHCb Collaboration 26

4 The LHCb Detector **28**
4.1 Pseudo-rapidity . . . 28
4.2 Detector Layout . . . 29
4.3 Tracking . . . 30
4.3.1 VELO . . . 30
4.3.2 Silicon Trackers . . . 31
4.3.3 Outer Tracker and Straw Tube Technology . . . 34
4.3.4 Why Silicon Detectors over TPC? . . . 35
4.4 Particle Identifcation . . . 37
4.4.1 RICH . . . 37
4.4.2 Calorimeters . . . 38
4.4.3 Muon System . . . 40
4.4.4 Flavour Tagging . . . 40
4.5 Trigger . . . 43

5 LHCb Simulation Software **45**
5.1 Gauss . . . 45
5.2 Gaussino . . . 45

6 Setup and Detector Geometry **47**
6.1 ParticleGun . . . 47
6.2 Fast Calorimeter Simulation . . . 47
6.2.1 Why Calorimeter? . . . 48
6.3 CaloChallenge . . . 48
6.3.1 Geometry . . . 49
6.4 Setup . . . 50

7 Monitoring Plots of GEANT4 + AdePT vs GEANT4 **51**

8 Conclusion **59**

Chapter 1

Introduction

1.1 Simulation in High Energy Physics

In physics, simulations are indispensable tools for several reasons. Firstly, many physical phenomena, especially at the subatomic level, are inherently probabilistic, governed by quantum mechanics. Secondly, even classically deterministic systems can be too complex to solve analytically. Simulations give us a way to explore these systems with numbers, showing us how they work. Also, simulations let physicists run "experiments" virtually. This helps when designing actual experiments, setting up detectors just right, and checking if theories work. Simulations can also test extreme conditions or "what if" scenarios we can't recreate in labs. Lastly, looking at simulated data alongside real experimental data helps us understand physics better and separate actual signals from background noise. Basically, simulations connect theory with experiment, helping us learn more about the universe.

1.2 Monte Carlo Simulation

Monte Carlo simulation is a powerful computational technique that utilizes random numbers to model and analyze complex systems. Instead of seeking exact analytical solutions, which are often intractable for certain problems, Monte Carlo methods generate numerous random samples and use statistical analysis to approximate the desired outcome. The underlying principle is to represent uncertainties or probabilistic aspects of a system through probability distributions. Random numbers are then drawn from these

distributions, and the model is run repeatedly, each time with a different set of random inputs. The collection of results from these simulations provides a distribution of possible outcomes, allowing for the estimation of averages, probabilities, and uncertainties. To help understand what Monte Carlo methods essentially are, a detailed approach is given in **Appendix A**, and a simple example of a Monte Carlo simulation is explained in **Appendix B**.

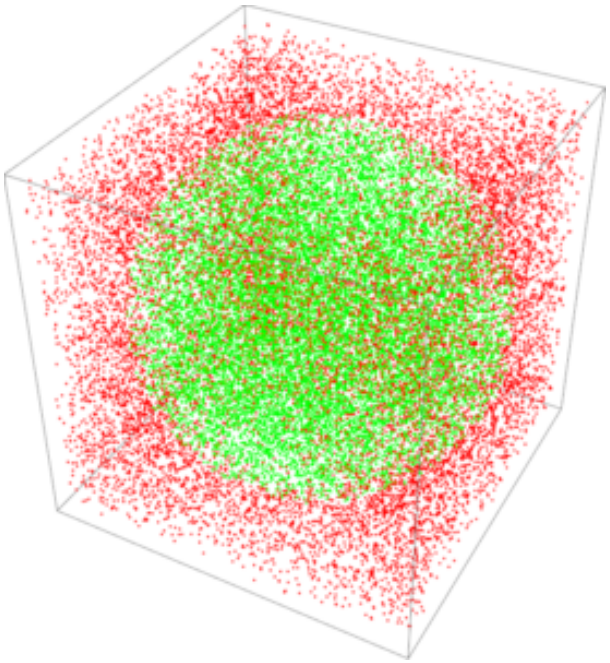


Figure 1.1: Randomly sampling points in n-dimensional spheres to find the formula for volume of n-sphere. See **Appendix A**.

1.2.1 Event Generation

Event generation in particle physics is a crucial process that involves simulating particle interactions and decays using sophisticated computer programs. These simulations, often referred to as Monte Carlo [12] event generators, are essential for designing experiments, understanding detector performance, and interpreting experimental data. Event generation starts with theoretical models that describe particle interactions based on the Standard Model of particle physics or theories beyond it. These models provide the fundamental laws and probabilities governing how particles interact and decay. These theoretical calculations often involve complex quantum field theory calculations, which are simplified using approximations and algorithms to make them computationally tractable. Due to the probabilistic nature of particle interactions, Monte Carlo methods are em-

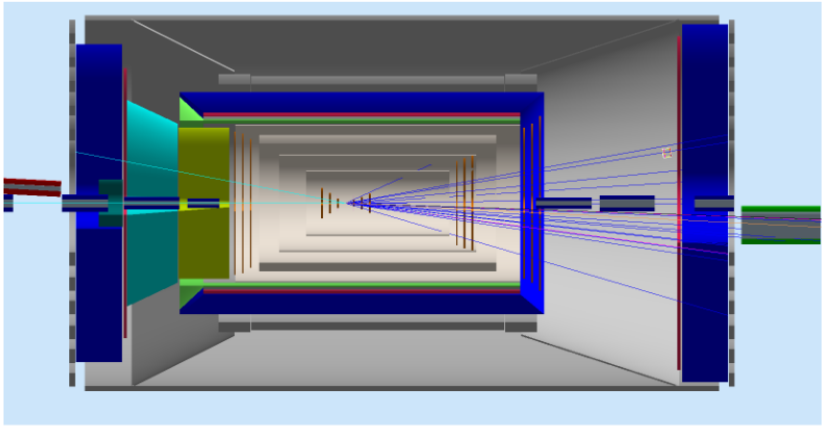


Figure 1.2: PYTHIA event display in Medium-energy Electron-Ion Collider at Jefferson Lab

ployed to simulate events. These methods involve generating random numbers to sample from probability distributions that describe various aspects of the interaction, such as the type of interaction that occurs, the momenta and energies of the outgoing particles and the decay products of unstable particles. Several sophisticated software packages, known as event generators, have been developed to perform these simulations. Some of the most widely used event generators in high-energy physics include

- **PYTHIA**: Focuses on general-purpose event generation, including hard and soft QCD processes, parton showers, and hadronization.
- **MadGraph**: Primarily used for generating matrix elements for specific processes.

Event generation typically proceeds through several key stages. It begins with the "hard process," simulating the fundamental interaction between colliding particles, such as the production of new particles or scattering. After the initial collision, we model what's called the "parton shower" - basically tracking how quarks and gluons cascade into streams of additional particles. Then comes "hadronization," where these fundamental particles cluster together to form composite particles (hadrons). The simulation also tracks how unstable particles decay based on their known behaviors and lifespans. All this generates a comprehensive list of particles with their properties, which we can then feed into a detector simulation to see how real equipment would respond to these events.

1.2.2 Detector Simulation and Particle Transport

Detector simulation is absolutely crucial in particle physics - it's the bridge connecting our theoretical models with what we actually measure in experiments. We simulate how particles travel through the complex materials and components of our detectors, replicating all the physics interactions that would happen in real life. This gives us simulated detector signals that are invaluable for multiple reasons. Before building expensive equipment, we use these simulations to optimize detector designs - tweaking geometry, materials, and electronics to get the best performance for our physics goals. The simulations help us understand exactly how different particles interact with detector components and generate signals. They're also essential for estimating background noise that might mimic our signals of interest, which is critical when determining if a result is significant. By comparing what our simulations predict with actual experimental data, we can test theoretical models and extract meaningful physics parameters. The gold standard software tool for this kind of simulation in high-energy physics is **GEANT4 (GEometry ANd Tracking 4)**, which provides incredibly detailed modeling capabilities.

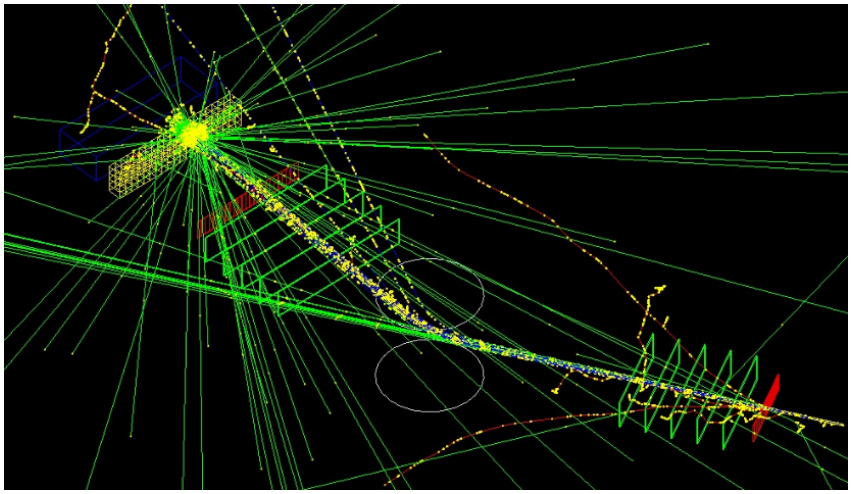


Figure 1.3: GEANT4 Simulation of a Double Arm Spectrometer

1.3 GEANT4

It is a general-purpose Monte Carlo simulation toolkit that simulates the passage of particles through matter. The detector's geometry, including the shape, size, and position of all its components (detectors, magnets, support structures, etc.), is precisely defined

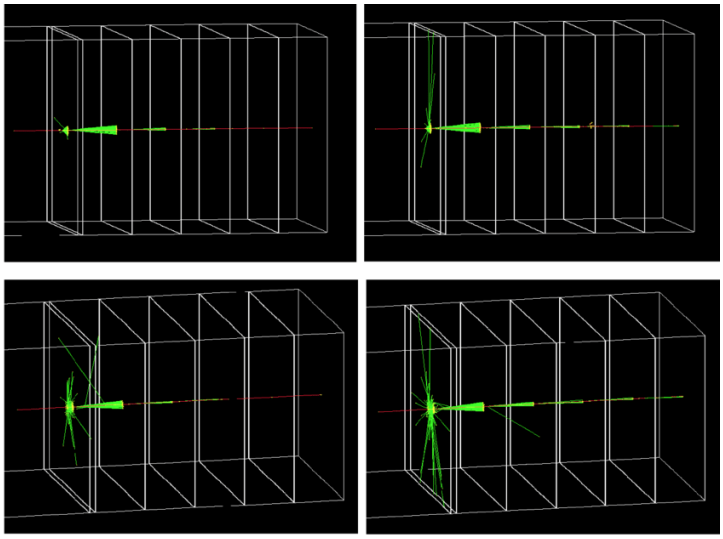


Figure 1.4: GEANT4 Simulation of Cherenkov Radiation

in the simulation. The materials used in the detector are defined, including their density, composition, and relevant physical properties (e.g., radiation length, interaction length). GEANT4 includes a wide range of physics models that describe the interactions of particles with matter, including:

- Electromagnetic interactions: Ionization, Bremsstrahlung, Compton scattering, Pair Production.
- Hadronic interactions: Elastic and inelastic scattering, particle production.
- Decays: Decay of unstable particles.
- Optical processes: Cherenkov radiation, scintillation.

The simulation tracks the particles as they move through the detector, simulating their interactions with the detector material step by step. The simulation models the generation of signals in the detector components, such as energy deposition in calorimeters, ionization in gaseous detectors, light emission in scintillators and electronic signals in readout systems.

1.4 Geometry Description Markup Language (GDML)

Geometry description is a key component of simulation applications, often making implementation complex and time-consuming. It is frequently needed across multiple applica-

tions, including different simulation engines, visualization, reconstruction, and analysis. Since each application has its own geometry format, users must either reimplement geometries or create conversion mechanisms. Many opt for custom XML-based [19] formats for flexibility and reuse in event processing. However, this approach tightly integrates geometry with experimental frameworks, limiting its use in standalone applications. To solve this, the **Geometry Description Markup Language (GDML)** was developed as an **XML**-based, application-independent solution. XML offers easy reading, writing, and extensibility, making it widely applicable. Markup languages are perfect for describing geometry, and one of the great things about GDML files is you can edit them with any basic text editor. This makes sharing geometry setups between different simulation and analysis tools much smoother, boosting both compatibility and workflow efficiency.

1.4.1 GDML Schema

When we talk about a GDML schema, we're referring to an **XML Schema Definition (XSD)** [19] file that essentially sets the rules for how Geometry Description Markup Language files should be structured. It's like a rulebook that ensures all GDML files follow consistent formatting, which means parsers in programs like Geant4 can properly understand and work with them without running into issues. The schema specifies:

- Allowed elements and attributes (e.g., <materials>, <solids>, <volume>)
- Data types (e.g., numbers, strings, units)
- Hierarchical relationships (e.g., how volumes contain other volumes)

By validating a GDML file against the schema, users can detect syntax errors and ensure compatibility with simulation tools.

Structure (Figure 5)

1. The first section, '**define**', contains numerical values for various constants, positions, and rotations that will be referenced later during geometry construction.
2. The second section, '**materials**', defines all materials used in the geometry. It supports both simple materials (composed of a single element) and mixtures, which can be specified based on mass fraction or atomic composition.



Figure 1.5: GDML File

3. The third section, '**solids**', includes all solid shapes used in the geometry description. Supported shapes include box, sphere, tube, cone, polycone, parallelepiped, trapezoid, torus, polyhedra, hyperbolic tube, elliptical tube, and ellipsoid, with new shapes continuously added. Additionally, composite solids created through Boolean operations (union, subtraction, intersection) are supported.

4. The fourth section defines the actual geometry tree, assigning solids and materials to different volumes. The hierarchy is established by positioning daughter volumes (**physvol**) within parent volumes. The structure supports assembly volumes, reflections, replicas, and divisions, along with basic support for parameterized volumes, which will be expanded in future updates.

5. The final section, '**setup**', specifies the top volume of the geometry tree. Multiple setups can be defined within a single file, enabling the testing of different subcomponents or configurations without modifying the GDML file.

1.4.2 GDML Reader and Writer

A GDML Reader parses (converting data from a file format to data structures within a programming language) and processes GDML files, extracting materials, solids, volumes, and transformations for simulations like Geant4. It validates the file against the GDML schema, stores data in structured formats, and converts it into simulation objects. Geant4's G4GDMLParser [19] automates geometry setup, while ROOT can visualize GDML geometries. The reader applies transformations, ensuring correct positioning. Custom readers in Python (ElementTree, lxml) or C++ further enhance usability. GDML Readers ensure consistency, automation, and efficiency in physics simulations, reducing manual setup while enabling geometry reuse across applications. This makes them crucial for accurate detector modeling.

A GDML Writer generates GDML files by exporting geometry definitions, materials, solids, and transformations into XML format for use in simulations like Geant4. It converts in-memory simulation objects into structured GDML elements, ensuring compatibility with the GDML schema. Geant4's G4GDMLParser supports writing geometries, while ROOT and custom Python (ElementTree, lxml) or C++ implementations allow flexible exporting. GDML Writers enable geometry reuse, consistency, and automation, making them essential for sharing and modifying detector models without manually redefining them. This facilitates efficient geometry management across simulations, visualization, and analysis applications.

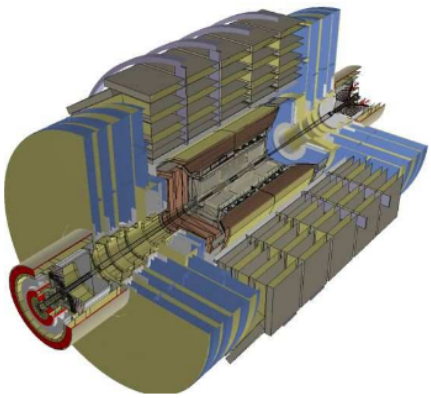


Figure 1.6: CMS detector visualized using ROOT from an automatically generated GDML file.

1.5 AdePT

AdePT (Accelerated demonstrator of electromagnetic Particle Transport) is a collaborative R&D project dedicated to accelerating electromagnetic particle transport simulations, a computationally intensive bottleneck in high-energy physics. These simulations are crucial for detector design, background estimation, and data interpretation, but simulating electromagnetic showers (from electrons, positrons, and photons) is particularly demanding. AdePT addresses this by leveraging the parallel processing power of GPUs. The project aims to develop a high-performance GPU-based transport engine, optimizing data structures (like Array of Structures) and algorithms for GPU architectures. Adapting and optimizing existing GEANT4 physics models for efficient GPU execution is a key focus, requiring code rewriting and careful memory management. Efficient geometry handling is also crucial, with AdePT developing GPU-friendly geometry representations and navigation algorithms to minimize data transfer between CPU and GPU [2] [1]. Several challenges are being tackled, including efficient data handling and GPU memory management, optimized kernel scheduling for maximum GPU performance, and the potential use of single-precision floating-point arithmetic for speedup while maintaining acceptable accuracy. AdePT is not intended to replace GEANT4 but rather to provide a GPU-accelerated component for integration or standalone use. The potential benefits are substantial: significant speedups in electromagnetic shower simulations, enabling more detailed and complex studies. This enhanced performance facilitates a deeper understanding of detector behavior and fundamental physics, ultimately aiding in the design and analysis of future high-energy physics experiments facing ever-increasing computational demands.

1.6 Purpose of the Research

The future LHC runs and upgrades will require the experiments to simulate a larger number of events in order to provide enough statistics to reach the expected accuracy of the physics analysis. One potential way of achieving this is by exploiting GPU-based computing resources. The development of the GPU-based simulation prototype for electromagnetic physics called AdePT (Accelerated demonstrator of electromagnetic Particle

Transport) has reached the stage where all the necessary ingredients (physics, geometry, scheduling) for detector simulation are available. The next step is to integrate this prototype into the **Gaussino** simulation framework by providing all the necessary interfaces. This will demonstrate the use of AdePT in the LHCb simulation setup. The main goal of the project is to explore the interfacing between GEANT4 and AdePT and to see how (and how efficiently) this can be used in concrete applications like **Gauss**. We will discuss further about Gauss and Gaussino in sections **6** and **7**.

Why AdePT?

[1] Why AdePT, and why not just modify GEANT4 directly for GPUs? It boils down to a mix of complexity, maintainability, and performance optimization strategies. GEANT4 is a massive and complex codebase. Rewriting large portions of it to be GPU-compatible is a monumental task. It would require a huge amount of effort and expertise, and it would be very difficult to ensure that all the changes were correct and didn't introduce new bugs. The risk of destabilizing the entire GEANT4 framework was significant. Modifying GEANT4 directly for GPUs would create two separate versions: one for CPUs and one for GPUs. This would significantly increase the maintenance burden. Any bug fixes or improvements would have to be implemented in both versions, doubling the work. Keeping the two versions synchronized and ensuring consistency would be a major challenge. GPU architectures are very different from CPU architectures. Code that performs well on a CPU might not perform well on a GPU, and vice versa. Optimizing code for GPUs requires specialized knowledge and techniques. It's often more efficient to develop a separate GPU-optimized component (like AdePT) that can be tightly integrated with GEANT4, rather than trying to adapt the entire GEANT4 codebase.

Why and which aspects of EM physics?

Electromagnetic interactions, and the resulting showers, are particularly computationally expensive to simulate. They involve a large number of individual interactions (ionization, bremsstrahlung, Compton scattering, pair production) that need to be tracked for many particles. This makes EM physics a prime target for GPU acceleration, as it represents a significant bottleneck in the overall simulation process. The calculations involved in simulating EM showers are often independent of each other. [20] **Why are these cal-**

culations independent? Once a particle is created, its interactions are self-contained and don't directly depend on other particles. The shower's energy is deposited over many detector cells, allowing separate calculations for each region. Some examples are Bremsstrahlung ($e^- \to e^- + \gamma$), Compton Scattering ($\gamma + e^- \to \gamma' + e^{-'}$) and Pair Production ($\gamma \to e^+ + e^-$). This makes them well-suited for parallel processing on GPUs, where many calculations can be performed simultaneously. Other physics processes, like hadronic interactions, might have more complex dependencies that make them harder to parallelize efficiently. While LHCb studies all kinds of physics, its flagship measurements related to CP violation and rare decays often involve EM particles (photons, electrons) in the final state. Accurate and efficient simulation of these EM particles is therefore crucial for these specific analyses. we'll learn more about CP violation in section **3**.

It's beneficial to have a basic understanding of particle detectors before we delve into the core of our discussion. Therefore, as a preliminary step, I would like to provide some background information on these crucial instruments. We'll begin by exploring the concept of detectors in general, starting from the basic cloud chamber to modern general-purpose detectors. Then we will shift out focus to the LHCb detector, which, unlike ATLAS and CMS, searches and studies a particular area of HEP. Finally we'll move on to the simulation software used in LHCb and discuss about the results on the integration of AdePT into Gaussino.

Chapter 2

What is a Detector?

Particle detectors are sophisticated scientific instruments designed to detect, track, and identify subatomic particles, such as those produced in particle accelerators or from cosmic rays. They are essential tools in particle physics, nuclear physics, and other fields that study the fundamental constituents of matter and their interactions. Particle detectors rely on the interactions of particles with matter. When a particle passes through a material, it can interact in various ways, such as ionization, excitation, scattering, Cherenkov radiation, etc.

The evolution of particle detectors is inextricably linked to our understanding of the fundamental building blocks of the universe. From simple observations with the naked eye to sophisticated electronic systems, the quest to visualize and measure subatomic particles has driven continuous innovation in detector technology.

In the nascent stages of particle physics, the human eye served as the first detector, observing scintillations [21] – flashes of light produced when radiation interacted with certain substances like zinc sulfide. This primitive method, though limited, led to the discovery of radioactivity. The advent of photographic plates marked a significant advancement, providing a permanent record of particle tracks imprinted on the emulsion. These plates were instrumental in early studies of cosmic rays and radioactivity.

The early to mid-20th century witnessed the rise of visualization techniques that allowed scientists to directly observe particle trajectories. The cloud chamber, invented by C.T.R. Wilson, created a supersaturated vapor where charged particles left visible trails of condensed droplets along their ionization paths. This ingenious device facilitated the discovery of the positron and the muon, revolutionizing our understanding of

fundamental particles. Nuclear emulsions, with their thicker emulsion layers, offered a three-dimensional record of particle interactions, proving crucial in the discovery of the pion and kaon. The bubble chamber, developed by Donald Glaser, utilized a superheated liquid where particle passage induced bubble formation, capturing particle tracks photographically. Bubble chambers played a pivotal role in the prolific discoveries of new particles during the 1960s and 70s, marking a golden age of particle physics.

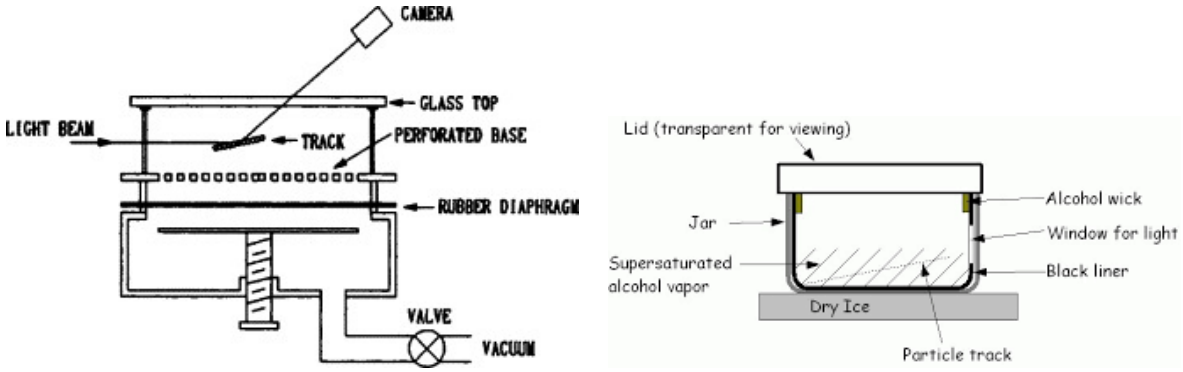


Figure 2.1: Bubble Chamber (left) and Cloud Chamber (right)

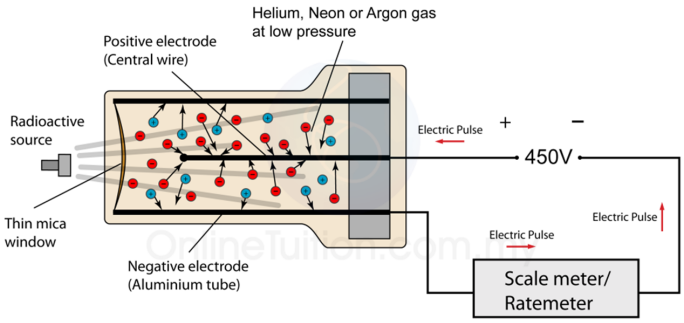


Figure 2.2: Geiger-Müller Counter

The mid to late 20th century ushered in the electronic revolution in particle detection. The Geiger-Müller counter, one of the earliest electronic detectors, measured ionization events in a gas-filled tube, generating electrical pulses. The combination of scintillating materials with photomultiplier tubes, which convert light into electrical signals, significantly enhanced detection sensitivity and precision. The spark chamber, employing closely spaced metal plates in a gas, visualized particle trajectories through electrical sparks. However, the true game-changer was the invention of the Multiwire Proportional Chamber (MPC) by Georges Charpak. These detectors, using arrays of thin wires to detect ionization, offered vastly improved spatial resolution and faster readout, paving

the way for modern high-energy physics experiments.

2.1 Scintillation Counter

Scintillation detectors mark a major leap forward in radiation detection, delivering better sensitivity and energy resolution than basic tools like Geiger-Müller (GM) tubes. These detectors work by transforming radiation energy into light, which then becomes an electrical signal we can measure. When radiation hits a scintillator (which could be an inorganic crystal like NaI or organic materials such as plastic) [21], it causes the material's atoms or molecules to become excited. This excitement creates a chain of energy transfers throughout the material, eventually reaching luminescence centers where the extra energy is released as light photons. What's key here is that the brightness of this light directly corresponds to how much energy the incoming radiation deposited.

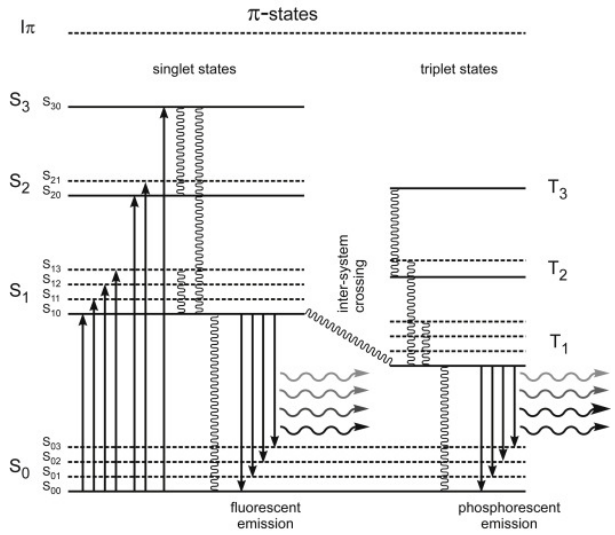


Figure 2.3: Electron Excitation in Scintillation Material

This light-producing process is what sets scintillation detectors apart from GM tubes, which work through direct gas ionization instead. In a GM tube, when radiation ionizes the gas inside, it triggers a massive electrical avalanche. While this gives us a simple way to count detection events, it tells us nothing about the energy of the radiation itself.

Scintillation detectors, by contrast, provide both event counts and energy information, making them suitable for spectroscopy and other applications requiring detailed radiation analysis.

The emitted light from the scintillator is typically very faint and requires amplifica-

tion to be useful. This is where the photodetector comes in. The scintillator is optically coupled to a photodetector, most commonly a photomultiplier tube (PMT). Optical coupling is achieved using a light guide or by directly attaching the scintillator to the PMT window with optical grease or adhesive to maximize light transmission.

A PMT operates on the principle of the photoelectric effect and secondary electron emission. Light photons from the scintillator strike a photosensitive surface (photocathode) within the PMT, releasing electrons through the photoelectric effect. These primary photoelectrons are then directed towards a series of dynodes, each held at a progressively higher positive voltage. When an electron strikes a dynode, it releases multiple secondary electrons. This process is repeated through multiple dynode stages, resulting in a significant amplification of the initial signal (typically $10^6 - 10^8$). The amplified signal is then collected at the anode, producing a measurable electrical pulse.

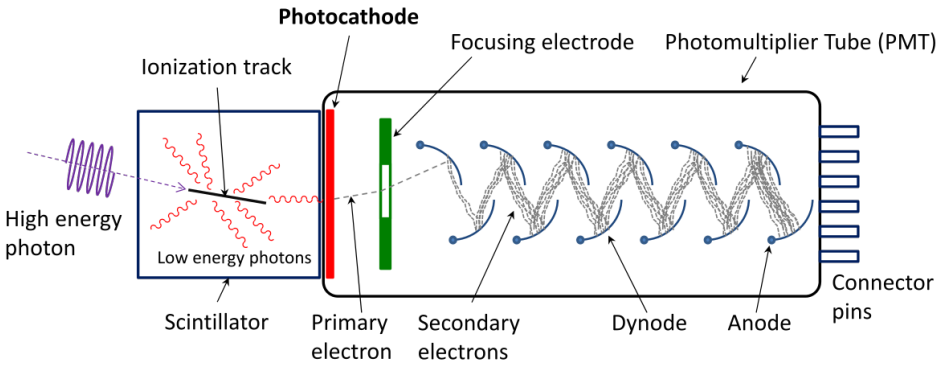


Figure 2.4: Scintillation Counter

The reason we need PMTs or similar photodetectors in scintillation detectors is that the light emitted by scintillators is extremely weak. Without amplification, it would be impossible to obtain a usable signal. PMTs provide the necessary gain to convert these faint light flashes into measurable electrical pulses, enabling precise detection and energy measurement of radiation. Modern detectors are also increasingly using Silicon Photomultipliers (SiPMs) which are semiconductor based and offer advantages like compactness and insensitivity to magnetic fields. This combination of scintillation and photoelectric amplification allows scintillation detectors to provide much more detailed information about radiation than simpler detectors like the GM tube.

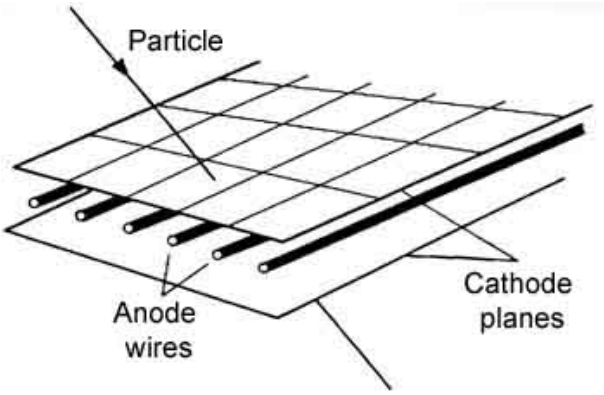


Figure 2.5: Multiwire Proportional Chamber

2.2 Multiwire Proportional Chamber

The Multi-Wire Proportional Chamber (MWPC) is a type of gaseous particle detector used to track the paths of charged particles. It consists of a chamber filled with a gas mixture, typically a noble gas like argon mixed with a quenching gas. Inside the chamber, a plane of thin, parallel anode wires is sandwiched between two cathode planes (either wires or solid plates). When a charged particle traverses the chamber, it ionizes the gas atoms along its path, creating ion-electron pairs. A positive voltage is applied to the anode wires, creating an electric field that causes the electrons to drift towards the anodes. As the electrons approach the thin anode wires, the electric field intensifies, leading to an avalanche of ionization. This avalanche amplifies the initial signal, producing a measurable electrical pulse on the anode wire. The key feature of the MWPC [21] is that the signal is proportional to the initial ionization, hence the "proportional" part of its name. This allows for energy loss measurements, providing some particle identification capabilities. The position of the particle can be determined by identifying which anode wire registered the signal. The spatial resolution is typically on the order of millimeters, limited by the wire spacing. A further development in MWPCs is the Time Projection Chambers and how it's used to reconstruct the track alongisde the energy deposition. Today TPCs are used as the main detector in modern detectors like STAR and ALICE. A short discussion on TPC will be helpful to appreciate the use of silicon detectors in LHCb.

2.2.1 Time Projection Chamber (TPC)

The Time Projection Chamber (TPC) stands as a testament to innovative detector design in particle physics, offering a comprehensive three-dimensional view of charged particle trajectories. It builds upon the principles of earlier gaseous detectors but significantly extends their capabilities to achieve superior spatial resolution, momentum measurement, and particle identification. The way a TPC works involves a complex mix of electric and magnetic fields, gas ionization, electron drift, and detailed electronic readout.

At its heart, the TPC contains a big volume of gas – usually a mix of a noble gas like argon or neon with a quenching gas such as methane or carbon dioxide. This gas serves as the detection medium. A steady electric field runs through this gas, created by a high-voltage cathode at one end and a segmented readout plane at the other. To keep this electric field uniform, specially positioned field-shaping rings or wires are placed inside the chamber. Many TPCs also use a strong magnetic field that runs parallel to the electric field. This magnetic field helps measure momentum by forcing charged particles into spiral paths – the tighter the spiral, the lower the momentum.

The detection starts when a charged particle moves through the TPC's gas. As it goes, the particle ionizes gas atoms, creating electron-ion pairs along its path. This is called "deposition" because the particle essentially leaves behind a trail of ionization. The uniform electric field then causes the negatively charged electrons to drift toward the readout plane. These electrons move at a constant, well-known speed – which is crucial for the TPC's accuracy. Simultaneously, the much heavier positive ions also drift, but their slower movement contributes negligibly to the fast signal.

The readout plane, a crucial component, is segmented into numerous individual pads or pixels. As the drifting electrons approach this plane, they induce small charges on the pads due to electrostatic induction. These induced charges are then measured by sensitive electronics connected to each pad. The amount of charge deposited on each pad, along with the precise time of signal arrival, forms the basis for track reconstruction.

The TPC's ability to reconstruct particle trajectories in three dimensions stems from this detailed charge measurement. The position of the hit pads on the readout plane directly provides two coordinates (x and y) of the particle's path. The third coordinate (z), along the direction of the electric field, is derived from the drift time of the electrons.

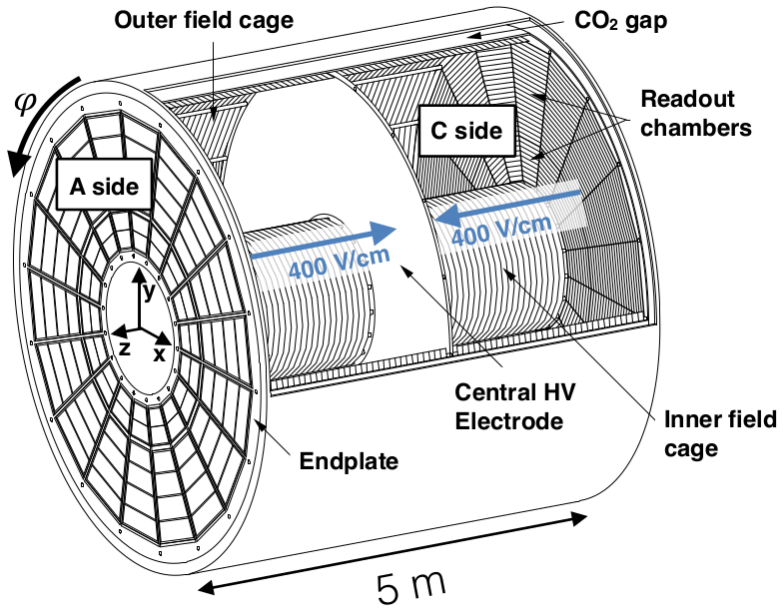


Figure 2.6: Time Projection Chamber

By multiplying the drift time with the known drift velocity, the distance the electrons traveled, and thus the z-coordinate of the ionization point, is determined. Combining the x, y, and z information from multiple pads allows for a precise reconstruction of the particle's three-dimensional trajectory. If a magnetic field is present, the curvature of this trajectory reveals the particle's momentum, with the direction of curvature indicating the particle's charge.

Beyond tracking, the TPC also provides valuable information about particle identification. The amount of ionization produced by a charged particle, quantified as energy loss per unit length (dE/dx), depends on the particle's charge and velocity. By measuring the charge deposited on the pads, the TPC effectively measures dE/dx. Combining this dE/dx information with the momentum measurement allows for particle identification, as particles with the same momentum but different masses will exhibit different dE/dx values.

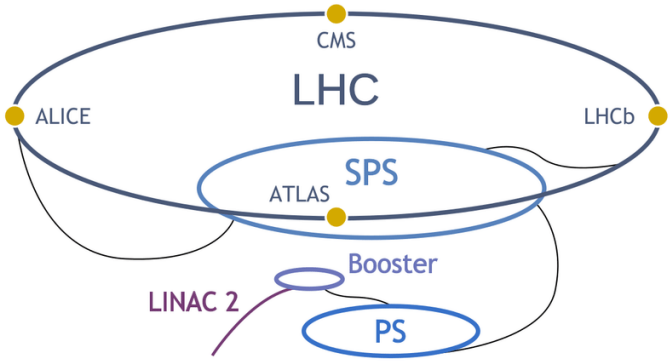


Figure 2.7: The Large Hadron Collider (LHC)

2.3 LHC and Modern Detectors

2.3.1 How does the LHC operate?

The Large Hadron Collider (LHC) accelerates protons to near the speed of light and collides them head-on, recreating conditions similar to those shortly after the Big Bang. These collisions provide physicists with a unique opportunity to study the fundamental constituents of matter and the forces that govern their interactions. The operation of the LHC, the organization of its interaction points, the production and detection of b hadrons by LHCb, and the rationale behind different data-taking "runs" are all intricately linked, forming a complex and fascinating story. The LHC accelerates protons in bunches, not as a continuous stream. These bunches, each containing billions of protons, circulate in opposite directions within the 27-kilometer ring. The beams are guided by powerful superconducting magnets, which maintain their circular trajectory. The collisions occur at specific locations around the ring called interaction points (IPs), where the two counter-rotating beams are brought together and focused by high-gradient quadrupole magnets to maximize the collision rate. There are four main IPs, each hosting a major experiment: IP1 (ATLAS), IP5 (CMS), IP2 (ALICE), and IP8 (LHCb) [23]. It's crucial to understand that collisions do not occur simultaneously at all four IPs in a continuous manner. Instead, the proton bunches are carefully timed and steered so that they cross at each IP at specific intervals. The frequency of these bunch crossings depends on the LHC's operating parameters, but they are typically very frequent, occurring millions of times per second at each IP. However, these are discrete events, not a continuous process. Imagine two circular

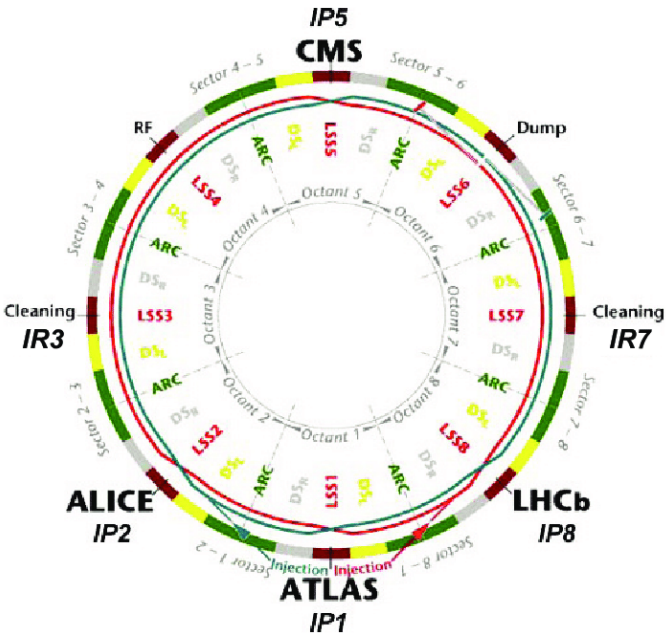


Figure 2.8: The four interaction points: IP1 (ATLAS), IP2 (ALICE), IP5 (CMS), IP8 (LHCb)

highways intersecting at four points. Cars (proton bunches) travel on these highways, and at each intersection, some cars might collide, but not all, and these collisions are not perfectly synchronized between intersections. This analogy illustrates how collisions occur at the LHC's IPs.

The LHC operates in distinct data-taking periods called "runs," separated by "long shutdowns" for maintenance and upgrades. These runs are essential for several reasons. Firstly, they allow for upgrades to the LHC accelerator itself, such as increasing the collision energy or the number of protons per bunch (luminosity). Secondly, the experiments at the IPs also undergo upgrades during the long shutdowns to improve their performance and cope with the changing conditions of the LHC. For example, LHCb underwent major upgrades during Long Shutdown 2 (LS2) to prepare for Run 3, which began in 2022. These upgrades were necessary to handle the increased luminosity of Run 3, which implies a higher rate of collisions and thus more data to process. Run 1 (2009-2013) saw collisions at 7 and 8 TeV, culminating in the discovery of the Higgs boson. Run 2 (2015-2018) increased the collision energy to 13 TeV, providing access to new physics processes. Run 3 (2022-2025) operates at 13.6 TeV with significantly increased luminosity, promising a wealth of new data and the potential for new discoveries. These different runs, with their varying energies and luminosities, are crucial for exploring different energy regimes and making precise measurements of rare processes.

2.3.2 General Purpose Detectors

At CERN, general purpose detectors play a crucial role in exploring the fundamental constituents of matter and the forces that govern them. The two largest general-purpose detectors at the LHC are the ATLAS and the CMS. ATLAS, a colossal detector at the Large Hadron Collider (LHC), probes fundamental questions in particle physics. Its primary goals include precise measurements of the Higgs boson, discovered in 2012 by ATLAS and CMS, and searches for new physics beyond the Standard Model, such as supersymmetry and dark matter. The detector's layered design features an inner tracker for charged particle trajectories, calorimeters for energy measurement of electrons, photons, and hadrons, and a muon spectrometer for muon identification. Its massive size, weighing 7,000 tonnes, and complex magnet system enable precise momentum measurements. ATLAS, through international collaboration and sophisticated data analysis, continues to explore the universe's fundamental constituents and forces.

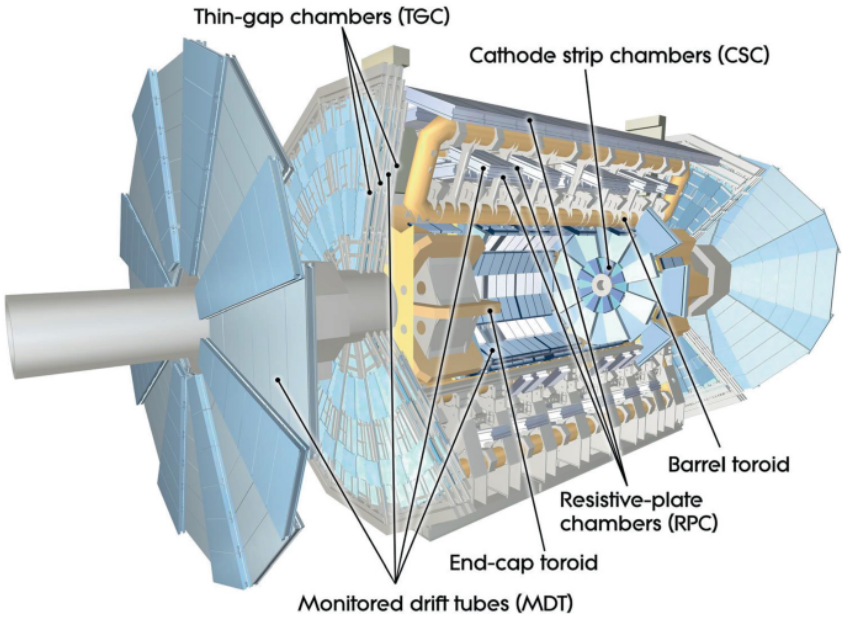


Figure 2.9: ATLAS Detector

CMS (Compact Muon Solenoid) is the other general-purpose detector at the Large Hadron Collider (LHC), designed to explore fundamental particle physics. Its key achievements include the co-discovery of the Higgs boson in 2012, confirming the existence of the Higgs field. CMS investigates phenomena beyond the Standard Model, such as dark matter and extra dimensions, and studies the properties of known particles like the top quark. Its design features a powerful superconducting solenoid magnet, enabling precise momen-

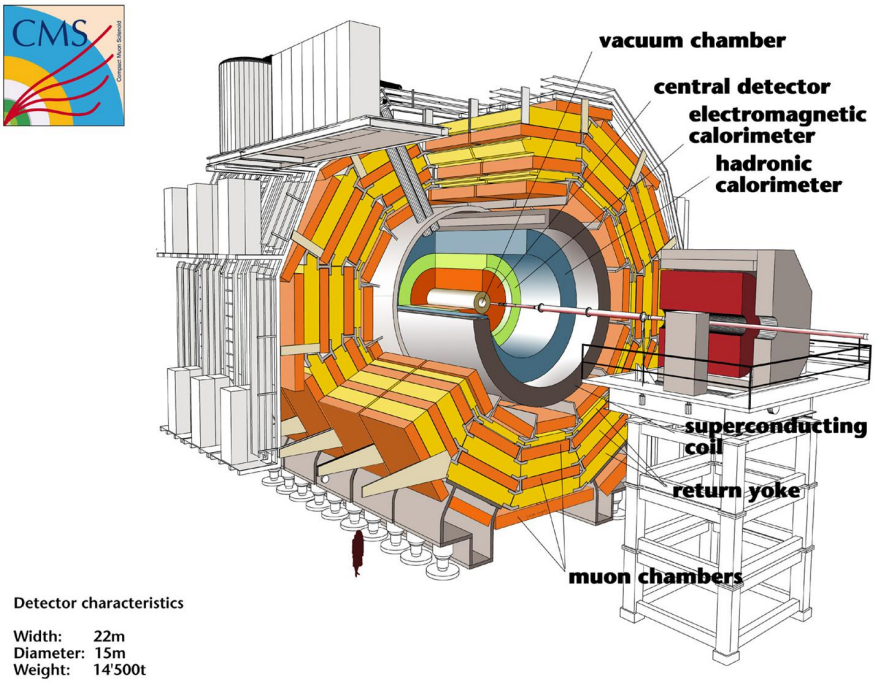


Figure 2.10: CMS Detector

tum measurements of charged particles. Inside, silicon trackers provide high-resolution tracking, while electromagnetic and hadronic calorimeters measure particle energies. The muon system, embedded within the magnet's return yoke, identifies and measures muons. CMS, through international collaboration and extensive data analysis, contributes significantly to our understanding of the universe's fundamental building blocks and forces.

Chapter 3

CP Violation and LHCb

3.1 Parity Violation

Parity (**P**) is a fundamental concept in physics that deals with the symmetry of physical systems under spatial inversion (**mirror reflection**). It helps us understand whether the laws of physics remain unchanged when all spatial coordinates $(\boldsymbol{x}, \boldsymbol{y}, \boldsymbol{z})$ are flipped to $(-x, -y, -z)$. Parity is essentially a mirror symmetry operation. If a system behaves the same way after flipping its spatial coordinates, it is said to be parity-even ($P = +1$). If the system behaves oppositely, it is parity-odd ($P = -1$). Newton's laws of motion and Maxwell's equations of electromagnetism are invariant under parity. This means they remain unchanged if we reflect all spatial coordinates. The electric field is a parity-even quantity and the magnetic field is a parity-odd quantity. Parity is conserved in strong and electromagnetic interactions but is violated in weak interactions, such as beta decay.

Wu's Experiment

Before 1956, parity (P) was assumed to be conserved in all fundamental interactions. However, in the early 1950s, physicists Tsung-Dao Lee and Chen-Ning Yang noticed inconsistencies in weak interaction decays. They proposed that the weak force might violate parity, especially in beta decay (the weak decay of neutrons into protons, electrons, and antineutrinos). To test this [15], Wu designed an experiment using polarized cobalt-60 nuclei.

Wu used a ^{60}Co source and placed it in a magnetic field along which the nucleus becomes polarized. The goal was to measure the rate of β^- from the decay:

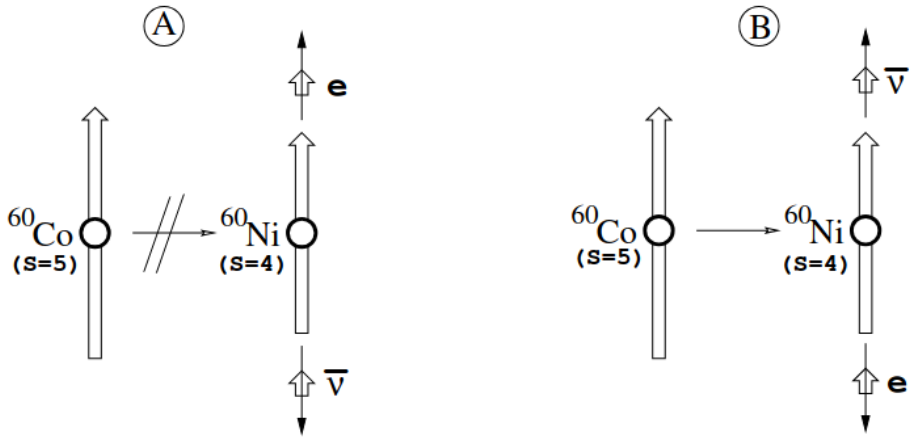


Figure 3.1: Probable transitions of ^{60}Co to ^{60}Ni. Open arrows denote spin while closed ones denote the momentum vector. (a) Forbidden transition [15]. (b) Allowed transition ; antineutrino is always **righthanded** (spin aligned with momentum vector).

$$^{60}_{27}\mathrm{Co} \rightarrow ^{60}_{28}\mathrm{Ni} + e^- + \bar{\nu}_e$$

in a small counter placed at small angles with respect to the field lines. By reversing the magnetic field, a deviation in the count rate could be detected. Experiment revealed that electrons were preferentially emitted opposite to the direction of the nuclear spin. This meant the weak interaction distinguished lefthanded from righthanded resulting in parity violation. If parity were conserved, flipping the coordinate system $(x, y, z \rightarrow -x, -y, -z)$ should not change the physics. However, the decay pattern was not symmetric after a parity transformation. This proved that the weak force violates parity.

3.2 Charge Conjugation Violation and CP Symmetry

Charge conjugation (**C**) symmetry is the idea that physics should remain unchanged if we replace all particles with their corresponding antiparticles. In other words, the laws of physics should be the same for a particle and its antiparticle with opposite charge. However, experiments have shown that the weak interaction violates charge conjugation symmetry, just like it violates parity (P).

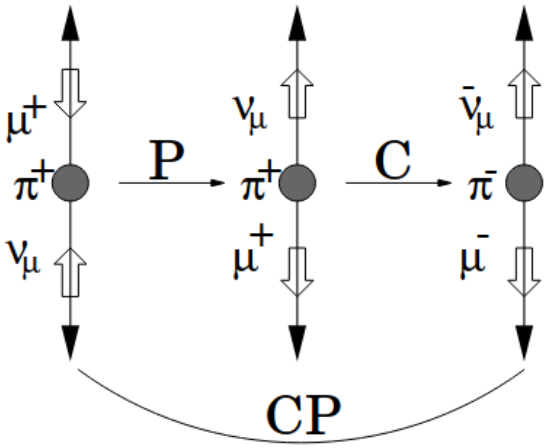


Figure 3.2: Action of C and P symmetry together preserving the underlying physics. [15]. Open arrows denote spin while the solid ones the momentum vectors.

A key test of charge conjugation symmetry [15] was performed using pion decay:

$$\pi^+ \rightarrow \mu^+ + \nu_\mu$$

Considering no changes to megnetic field direction (no parity transformation), after charge conjugation, we have an unphysical result as:

$$\pi^- \rightarrow \mu^- + \bar{\nu}_\mu$$

because antineutrinos exist as right-handed. But a combined parity and charge conjugation transformation (CP) results to an allowed process (Fig. 18). Therefore, the combined operation of parity and charge conjugation seems at leastg to provide a symmetery of nature.

3.3 CP Violation

One of the most famous and well-studied examples of CP violation comes from the neutral kaon (K^0) and its antiparticle ($\bar{K}^0$) system. This discovery was groundbreaking because it showed that the combined symmetry of Charge Conjugation (C) and Parity (P) is not perfectly conserved in weak interactions.

K^0 consists of down (d) and anti-strange ($\bar{s}$) quarks and $\bar{K}^0$ consists of anti-down ($\bar{d}$) and strange (s) quarks. In the weak interaction [15], these two particles mix to form two new quantum states:

1. K_S (short-lived state - decay quickly, $\sim 10^{-10}s$)

2. K_L (long-lived state - decays more slowly, $\sim 10^{-8}s$)

If CP symmetry is conserved, the decays of these states should follow strict rules:

1. K_S should decay into two pions ($\pi^+\pi^-$), a CP-even final state.

2. K_L should decay into three pions ($\pi^+\pi^-\pi^0$), a CP-odd final state.

In 1964, James Cronin and Val Fitch conducted an experiment that revealed a small fraction of K_L particles decayed into two pions:

$$K_L \rightarrow \pi^+ + \pi^-$$

This two-pion decay is CP-even, but K_L is supposed to be CP-odd. This means that CP symmetry is violated because a CP-odd particle is decaying into a CP-even final state. This discovery showed that the weak force favors matter over antimatter, providing a clue as to why our universe is dominated by matter instead of equal parts matter and antimatter. While CP violation in kaons is not large enough alone to explain the entire matter-antimatter asymmetry, it proves that the universe does not treat matter and antimatter equally. Ongoing research in CP violation, particularly in B-mesons, neutrinos, and leptogenesis models, may provide the missing pieces to explain why the universe is dominated by matter.

3.4 Objectives of the LHCb Collaboration

The LHCb experiment at CERN is uniquely positioned to investigate CP violation, with a specific focus on the decays of b hadrons (particles containing b quarks). The experiment's design is optimized for this purpose, boasting several key features. The LHC produces copious amounts of b quark-antiquark pairs, providing LHCb with the necessary statistics to study even rare decay processes. The detector itself is equipped with high-precision tracking and vertexing capabilities, allowing for the accurate reconstruction of b hadron decays, which is crucial for measuring CP violation parameters. LHCb's advanced particle ID system (including those RICH detectors) lets researchers tell different particles apart - which is crucial when you're studying specific decay patterns. They've really moved the

needle on CP violation research. Their super-precise measurements of CP violation in neutral B mesons (B^0 and B^s) have confirmed what the Standard Model predicted while drastically reducing measurement uncertainties. They didn't stop there - they've also seen CP violation happening in charged B meson decays, which puts even more constraints on the Standard Model. But what's really exciting is how LHCb is actively searching for new physics by looking for places where rare b decays don't match Standard Model predictions. Any discrepancies could point to new particles or interactions affecting CP violation beyond what we currently understand. One of their biggest breakthroughs was spotting CP violation in charm meson decays [14] - a huge deal since the Standard Model predicted only tiny CP violation in this area. This discovery opens up fresh avenues for exploring potential new physics. Here's the thing - while the Standard Model explains some CP violation, it can't account for the massive matter-antimatter imbalance in our universe. That's why these detailed CP violation measurements across different systems (especially in b hadron decays at LHCb) are so important. This work is essential for discovering physics beyond the Standard Model and building a more complete picture of the fundamental forces and particles that make up our universe. Claude can make mistakes. Please double-check responses.

Chapter 4

The LHCb Detector

4.1 Pseudo-rapidity

A quantity called rapidity, y, is Lorentz invariant under boosts along the beam axis. This means that if you change your frame of reference by moving along the beam direction, the difference in rapidity between two particles remains the same. This is extremely useful for studying particle production, as the physics processes should be independent of the boost of the colliding partons. The expression for rapidity is as follows:

$$y = \frac{1}{2} \ln[(E + p_z)/(E - p_z)] \tag{4.1}$$

where, p_z is the momentum of the particle in the beam direction and E is the energy. Pseudorapidity is an approximation of rapidity, defined as:

$$\eta = -\ln[\tan(\theta/2)] \tag{4.2}$$

where θ is the angle between the particle's momentum and the beam axis. For highly relativistic particles (where the particle's energy is much greater than its mass, which is often the case at the LHC), pseudorapidity becomes very close to rapidity. For massless particles (like photons), they are exactly equivalent. A detailed derivation of pseudorapidity is given in **Appendix B**. Pseudorapidity only depends on the angle θ, which is easily measurable in detectors, whereas, rapidity, on the other hand, requires knowledge of the particle's energy or momentum, which explains the use of pseudorapidity in high energy physics. In hadron collisions, particle production is approximately uniform in ra-

pidity (and therefore approximately in pseudorapidity). This means that if you plot the number of particles produced as a function of pseudorapidity, you get a roughly flat distribution in the central region. This is very convenient for detector design and analysis, as it means that the detector acceptance can be easily defined in terms of pseudorapidity. It has a direct relationship with the geometry of detectors. Detectors are often designed with a constant coverage in pseudorapidity. This means that the detector elements are arranged in such a way that they cover a fixed range of η. This simplifies the design and construction of detectors, as it ensures that the detector has a uniform response to particles produced at different angles.

LHCb's pseudorapidity range of 2 to 5 is chosen to optimize the detection of b hadrons, which are produced predominantly at small angles (forward direction). This range corresponds to an angular coverage of approximately 0.77 to 15.4 degrees relative to the beam axis. The formula $\eta = -\ln[\tan(\theta/2)]$ allows for the conversion between pseudorapidity and angle.

4.2 Detector Layout

The LHCb detector is designed as a single-arm spectrometer that covers a forward angular range of approximately 10 to 300 mrad [17] [11] in the bending plane and 10 to 250 mrad in the non-bending plane. This specific geometry was chosen because at high energy collisions, both b-hadrons and their antiparticles are primarily produced within the same forward or backward cone, making this focused coverage highly efficient. The detector's beam-pipe includes the VELO's forward window (which covers the entire LHCb acceptance range) along with four main conical sections. The three sections closest to the interaction point are constructed from beryllium, while the farthest section is made of stainless steel. Unlike ATLAS and CMS which have a roughly cylindrical or barrel-shaped layout, with detectors arranged in concentric layers around the interaction point, LHCb consists of a series of detectors placed along the beam pipe on one side of the interaction point. This configuration is optimized to detect particles produced at small angles relative to the beam direction (in the forward region), unlike the general purpose detectors which provide nearly full coverage in the plane perpendicular to the beam direction, allowing them to detect particles produced at a wide range of angles.

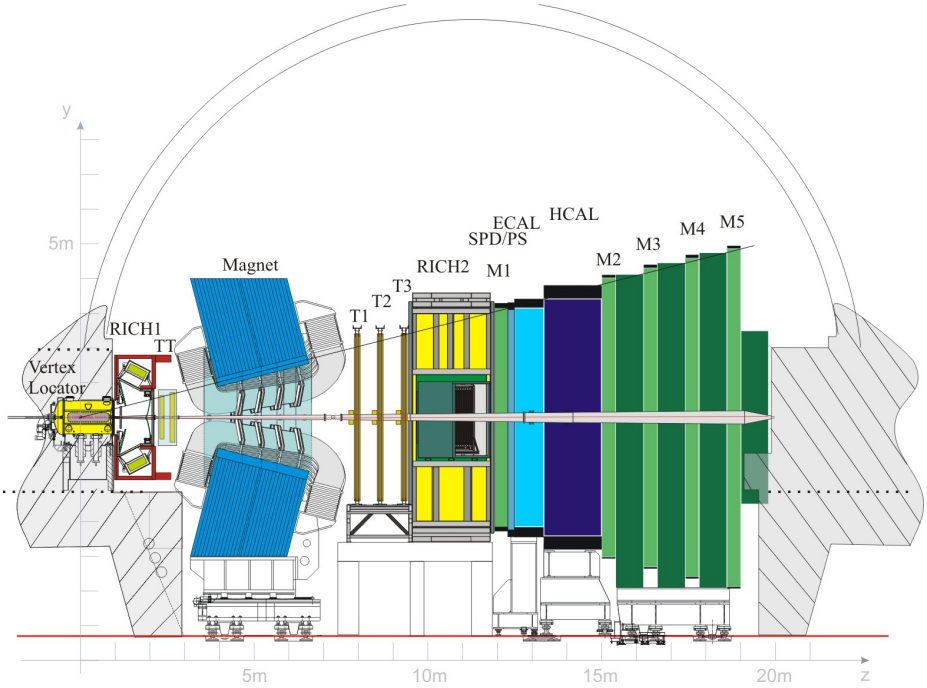


Figure 4.1: LHCb Detector Layout

4.3 Tracking

The LHCb tracking system is composed of the vertex locator system (VELO) and four planar tracking stations: the Tracker Turicensis (TT) positioned upstream of the dipole magnet and stations T1-T3 located downstream . Both the VELO and TT utilize silicon microstrip detector technology. In the T1-T3 stations, silicon microstrips are implemented in the area near the beam pipe (known as the Inner Tracker or IT), while straw-tube technology is employed in the outer regions of these stations (designated as the Outer Tracker or OT). The TT and IT components were developed as part of a unified project called the Silicon Tracker (ST).

4.3.1 VELO

The VELO is designed to precisely measure the decay vertices of particles, particularly those containing b quarks (b-hadrons). When protons collide in the LHC, b-hadrons are produced and travel a short distance before decaying into other particles. The VELO measures the origin of these b-hadrons (primary vertex) [17] [11] and the point where they decay (secondary vertex) with very high accuracy. This precise vertexing is essential for studying the properties of b-hadrons, including their lifetimes, decay modes, and CP

violation (matter-antimatter asymmetry). The VELO is positioned very close to the LHC beam interaction point, only a few millimeters away. This proximity is crucial for achieving the required precision in vertex measurement, as b-hadrons travel only a very short distance before decaying. The VELO consists of two halves that are retracted during beam injection and then moved into their operational position close to the beam once stable beam conditions are established. This retractable design protects the delicate sensors from damage during injection.

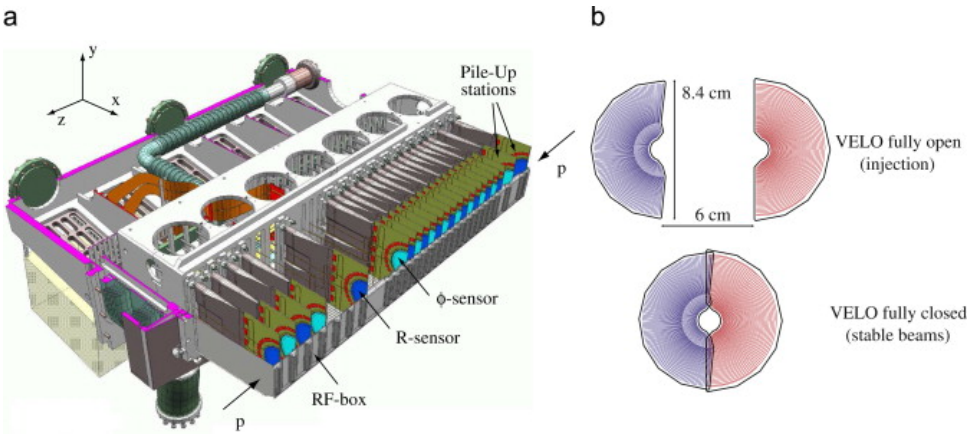


Figure 4.2: VELO Silicon Sensors

When the LHC starts up or after maintenance periods, the proton beams are injected into the accelerator and gradually accelerated to their operational energy. During this process, the beam conditions are unstable, meaning the beam position, intensity, and focus can fluctuate significantly. If the VELO were in its operational position (very close to the beam) during these unstable periods, it could be directly hit by the beam. This would cause severe damage to the delicate silicon sensors, which are extremely sensitive to radiation and direct impacts. To prevent this, the VELO is designed to be retractable. It consists of two halves that are initially positioned away from the beam pipe. Once the LHC achieves stable beam conditions and the beam is safely confined within its designated path, the VELO halves are moved inwards to their operational position, just a few millimeters from the interaction point.

4.3.2 Silicon Trackers

Silicon detectors offer excellent spatial resolution, allowing for precise determination of particle trajectories. This is crucial for reconstructing particle decays and measuring

their properties. When a charged particle passes through the silicon, it ionizes the silicon atoms, creating electron-hole pairs. These charge carriers are then collected by the strips, producing a signal that indicates the particle's passage. By combining the information from the VELO and the tracking stations, the trajectories of charged particles can be reconstructed with high precision. The bending of charged particle tracks in the LHCb magnet, combined with the track information from the silicon trackers, allows for precise momentum measurement.

In the LHCb experiment, the Silicon Tracker (ST) is a critical component consisting of two key detectors [17] [11]: the Tracker Turicensis (TT) and the Inner Tracker (IT). Both utilize silicon microstrip sensors with a precise strip pitch around 200 micrometers. The TT is a large, flat tracking station positioned upstream of the LHCb's dipole magnet, spanning 150 cm wide and 130 cm high. It provides essential track information for the Level-0 trigger, helping scientists identify fascinating collision events worth deeper investigation. Meanwhile, the Inner Tracker forms a cross-shaped region 120 cm wide and 40 cm high, situated downstream of the magnet. Each ST station incorporates four detection layers arranged in a strategic (x-u-v-x) configuration. The first and last layers feature vertical strips, while the middle layers have strips angled at -5° and $+5^{\circ}$ to enable precise spatial reconstruction. The TT boasts an impressive 8.4 $\mathbf{m^2}$ active area with 143,360 readout strips, some extending up to 38 cm. The IT covers 4.0 $\mathbf{m^2}$ with 129,024 readout strips varying between 11 and 22 cm in length. The detector's modular design is ingenious: half-modules cover specific acceptance regions, with readout hybrids strategically positioned. Full modules, assembled from two half-modules, ensure comprehensive coverage, with subtle staggering between adjacent modules preventing detection gaps and facilitating precise alignment.

The TT utilizes silicon microstrip detectors, and a key component of its design is the "4-2-1" module. This specific module type is implemented to effectively handle the varying particle flux encountered across the detector area. The "4-2-1" module is constructed from seven silicon sensors arranged in a linear fashion. These sensors, made from silicon wafers with etched microstrips, detect the passage of charged particles by registering the ionization they cause within the silicon. This ionization creates electron-hole pairs, which are then collected by the strips, generating an electrical signal. The unique aspect of the "4-2-1" module lies in how these sensors are divided into readout

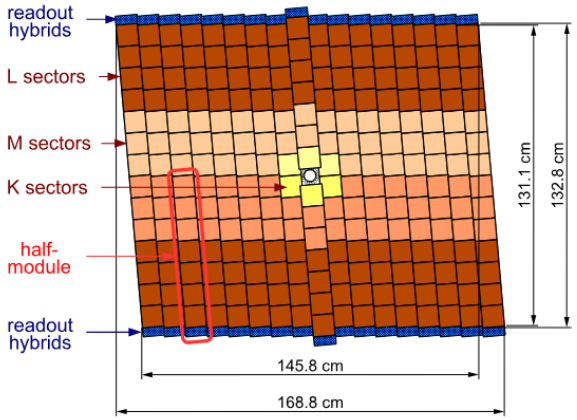


Figure 4.3: Layout of the third TT detection layer. Different readout sectors are indicated by different shadings.

sections. To address the challenge of increasing particle flux closer to the beam pipe, the seven sensors are grouped into three distinct readout sections with varying strip lengths. The "L" section, containing four sensors, is the longest and is positioned furthest from the beam pipe where particle density is lower. Closer to the beam pipe, where the flux increases, lies the "M2" section, comprising two sensors. Finally, the "K" section, consisting of a single, shortest sensor, is located closest to the beam pipe, designed to handle the highest particle flux.

This "4-2-1" designation directly reflects the number of sensors within each readout section: four in the L section, two in the M2 section, and one in the K section. This arrangement optimizes the detector's performance by providing finer segmentation in regions of higher particle flux. Each of these readout sections has dedicated readout electronics, enabling efficient signal processing even in high-occupancy areas. This variable strip length and dedicated electronics are crucial for maintaining efficient data acquisition and trigger performance. Silicon detectors offer excellent spatial resolution, allowing for precise determination of particle trajectories. This is crucial for reconstructing particle decays and measuring their properties. When a charged particle passes through the silicon, it ionizes the silicon atoms, creating electron-hole pairs. These charge carriers are then collected by the strips, producing a signal that indicates the particle's passage. By combining the information from the VELO and the tracking stations, the trajectories of charged particles can be reconstructed with high precision. The bending of charged particle tracks in the LHCb magnet, combined with the track information from the silicon

trackers, allows for precise momentum measurement.

4.3.3 Outer Tracker and Straw Tube Technology

Straw tube detectors are a widely used technology in particle physics for tracking charged particles, offering a compelling combination of performance, cost-effectiveness, and robustness. The detector's fundamental element is a thin-walled tube, often constructed from multiple layers of thin plastic film like Mylar, with an outer conductive coating serving as the cathode. A thin anode wire, typically made of tungsten, is strung along the tube's central axis. The tube is filled with a gas mixture, typically a noble gas like argon combined with a quenching gas. The detection mechanism hinges on gas ionization. When a charged particle passes through the straw tube, it interacts with the gas atoms, dislodging electrons and creating electron-ion pairs. An applied positive voltage on the anode wire generates an electric field within the tube, causing the negatively charged electrons to drift towards the anode. As these electrons approach the thin wire, [17] [11] the electric field intensifies dramatically, accelerating the electrons and leading to an avalanche of further ionization through collisions with other gas atoms. This avalanche amplifies the initial signal significantly. The movement of these electrons induces a measurable electrical pulse on the anode wire, which is then processed by external electronics. Crucially, the time it takes for the electrons to drift to the wire (the drift time) is measured with high precision. Knowing the drift velocity of the electrons in the gas, this drift time allows for a precise determination of the particle's position perpendicular to the wire. This provides excellent spatial resolution, typically on the order of 100 micrometers. The thin walls of the straws also contribute to a low material budget, minimizing multiple scattering of particles. This, combined with the fast signal production and relatively low cost, makes straw tubes ideal for large-scale tracking systems like those found in the LHCb Outer Tracker.

The Outer Tracker (OT) is designed to track charged particles that traverse the detector outside the acceptance of the Vertex Locator (VELO) and Inner Tracker. Located downstream of the LHCb dipole magnet, the OT plays a vital role in reconstructing the trajectories of particles produced in proton-proton collisions, particularly those originating from the decay of b hadrons. The OT utilizes straw tube technology as its primary detection method. These straw tubes are thin-walled tubes filled with a gas mixture,

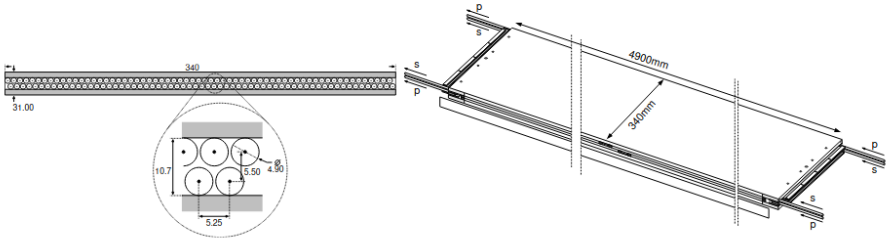


Figure 4.4: Cross section of a straw-tubes module (left) and overview of a straw-tubes module design (right).

typically argon and a quenching gas. When a charged particle passes through a straw tube, it ionizes the gas, generating a signal that allows for precise position measurement. The OT comprises approximately 55,000 such straw tubes, arranged in multiple layers to provide three-dimensional tracking information. The straws are organized into stations, each consisting of four layers. Two layers have their straws oriented horizontally (x-layers), while the other two are tilted at small angles (u and v layers), creating a stereo configuration. This x-u-v-x arrangement is essential for reconstructing particle tracks in three dimensions. The large surface area covered by the OT, approximately 360 m^2, ensures that a significant fraction of particles produced in the LHCb interaction point are tracked. The low material budget of the straw tubes minimizes multiple scattering, crucial for maintaining track precision, especially for high-momentum particles. The OT's combination of large coverage, precise tracking, and low material budget makes it an integral part of the LHCb experiment's physics program.

4.3.4 Why Silicon Detectors over TPC?

LHCb's primary goal is to study the decays of b hadrons, which have very short lifetimes and decay very close to the interaction point. To accurately reconstruct these decays and measure their properties, LHCb needs detectors with exceptional spatial resolution, fast readout, and high radiation hardness. Silicon detectors, particularly in the Vertex Locator (VELO) surrounding the interaction point, provide the necessary performance for this demanding task. While TPCs excel in high-multiplicity environments and provide particle identification capabilities through dE/dx measurements, the specific physics goals and experimental conditions of LHCb necessitate the superior spatial resolution and radiation tolerance offered by silicon technology.

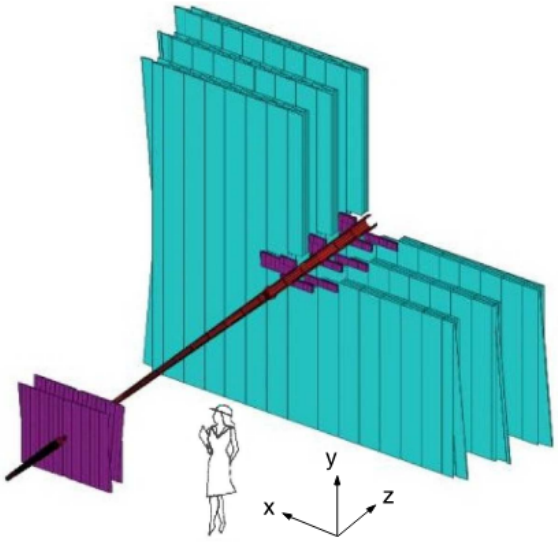


Figure 4.5: Arrangement of OT straw-tube modules in layers and stations

Silicon detectors exhibit significantly faster response times and can handle much higher data rates than TPCs. This is essential for coping with the LHC's high collision frequency, where millions of events occur per second. The fast signal collection in silicon allows for efficient data acquisition and minimizes pile-up effects (multiple events overlapping in time). TPCs, with their inherent drift time limitations, cannot match this speed. Silicon detectors provide unparalleled spatial resolution, reaching the micrometer scale (a few millionths of a meter). This precision stems from the short distances charge carriers travel within the silicon material. In contrast, TPCs, relying on electron drift in gas, have spatial resolution limited by diffusion, typically on the millimeter scale. This difference is critical for LHCb, where precise vertex reconstruction of short-lived b hadrons is paramount. Silicon detectors enable accurate determination of the decay point, crucial for studying CP violation and other rare decay processes.The environment near the LHC's interaction point is extremely harsh, with high levels of radiation. Silicon detectors can be designed to be highly radiation hard, maintaining their performance even after prolonged exposure. This is achieved through specific material processing and detector design techniques. TPCs, with their gas-filled volumes, are more susceptible to radiation damage, which can alter the gas properties and affect detector performance.

4.4 Particle Identifcation

4.4.1 RICH

Particle identification (PID) is crucial for the need to separate pions from kaons in certain B hadron decays. Having low transverse momenta at large polar angles and high transverse momenta at small polar angles, the particle identification system consistes of two Ring-Imaging Cherenkov (RICH) detectors to cover the full momentum range [17] [11]. When a charged particle surpasses the speed of light in a medium (like a gas, liquid, or solid), it polarizes the molecules of that medium. As the medium returns to its normal state, it emits photons of light, known as Cherenkov radiation. This light is emitted in a cone shape, with the particle's trajectory at the cone's apex. The medium through which the particle travels and emits Cherenkov radiation is called the radiator. RICH detectors can use different radiators depending on the momentum range of the particles they are designed to detect. The Cherenkov light emitted by the particle passes through the radiator and is then collected and focused by an optical system. This system typically consists of mirrors or lenses that direct the light onto a photon detector. The cone of Cherenkov light, when projected onto a planar detector, forms a ring or a disc. The radius of this ring is directly related to the angle of emission of the Cherenkov light, which in turn is related to the particle's velocity. By measuring the radius of the Cherenkov ring and knowing the particle's momentum (measured by other detectors in the experiment), the particle's velocity can be determined. Using the relationship between momentum, velocity, and mass, the particle's mass can be calculated, allowing for particle identification. In the LHCb experiment, two Ring Imaging Cherenkov (RICH) detectors play a crucial role in particle identification across different momentum ranges. RICH 1, positioned upstream of the magnet, is designed to detect low-momentum charged particles between 1-60 GeV/c using aerogel and C_4F_{10} radiators. It provides comprehensive coverage across the entire LHCb acceptance, spanning from ± 25 mrad to 300 mrad horizontally and 250 mrad vertically. RICH 2, located downstream of the magnet, focuses on high-momentum particles ranging from about 15 GeV/c up to and beyond 100 GeV/c. It employs a CF4 radiator and has a more focused angular acceptance of approximately ± 15 to ± 120 mrad horizontally and ± 100 mrad vertically, precisely targeting the region where high-momentum particles are

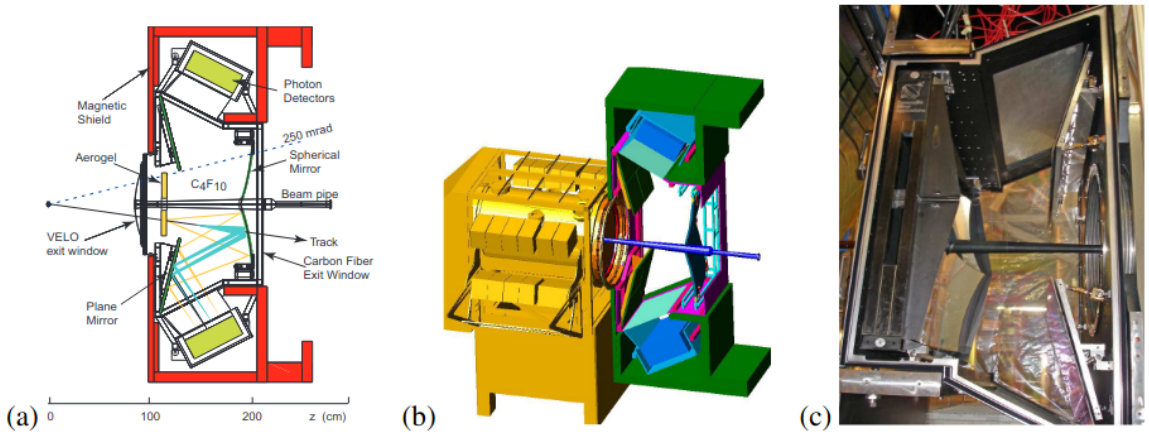


Figure 4.6: a) Side view schematic layout of the RICH 1 detector. (b) Cut-away 3D model of the RICH 1 detector, shown attached by its gas-tight seal to the VELO tank. (c) Photo of the RICH1 gas enclosure containing the flat and spherical mirrors. Note that in (a) and (b) the interaction point is on the left, while in (c) is on the right.

generated. Both RICH detectors utilize an innovative optical system with a combination of spherical and flat mirrors to redirect Cherenkov light away from the spectrometer's acceptance. The key difference lies in their optical layouts: RICH 1 features a vertical configuration, while RICH 2 adopts a horizontal approach.

4.4.2 Calorimeters

In the LHCb experiment, the calorimeter system is a multitasking powerhouse. Its primary role is to quickly identify and select potential hadrons, electrons, and photons during the first trigger level (L0), making critical decisions just 4 microseconds after particle collisions. Beyond rapid selection, the calorimeter does the heavy lifting of precisely identifying and measuring these particles' energies and spatial positions. This capability is crucial for the experiment's physics goals, especially when it comes to reconstructing specific particle interactions. Particularly important is the calorimeter's ability to accurately detect neutral pions (π_0) and prompt photons. These measurements are essential for flavor tagging and diving deep into B-meson decay studies, which are key components of the LHCb's research program. By providing such precise measurements, the calorimeter helps physicists unravel complex particle interaction mysteries. The LHCb calorimeter system consists of four main components [17] [11], arranged sequentially along the beamline. Scintillating Pad Detector (SPD) is the first detector in the calorimeter system. It's designed to quickly determine whether an incoming particle is charged or

neutral. It consists of scintillator pads that produce light when a charged particle passes through them. Photomultiplier tubes (PMTs) detect this light. The SPD provides a fast signal that is used in the Level-0 trigger. The Pre-Shower (PS) detector is located behind the SPD and is designed to distinguish between electrons and photons. It consists of a lead converter followed by scintillator pads. Electrons will start to produce electromagnetic showers in the lead, while photons will mostly pass through. The scintillator pads detect the charged particles from these showers. The PS provides information about the electromagnetic nature of the particle, which is used in the Level-0 trigger in conjunction with the ECAL. The Electromagnetic Calorimeter (ECAL) is designed to precisely measure the energy of electrons and photons. It's a "shashlik" type calorimeter, consisting of alternating layers of lead (absorber) and scintillator tiles. When an electron or photon enters the ECAL, it initiates an electromagnetic shower, producing a cascade of secondary particles. These particles excite the scintillator material, which emits light. The amount of light is proportional to the energy of the incident particle. The Hadron Calorimeter (HCAL) is designed to measure the energy of hadrons (particles made of quarks, such as protons, neutrons, and pions). It consists of alternating layers of iron (absorber) and scintillator tiles. When a hadron enters the HCAL, it initiates a hadronic shower, a cascade of secondary hadrons. These particles interact with the scintillator, producing light that is detected by PMTs. The information from all four components of the calorimeter system is combined to provide a comprehensive picture of the particles interacting with it. This information is used in the trigger system to select events of interest for further analysis. For example, a high-energy electron candidate would be identified by a signal in the SPD, a large signal in the PS and ECAL, and little to no signal in the HCAL.

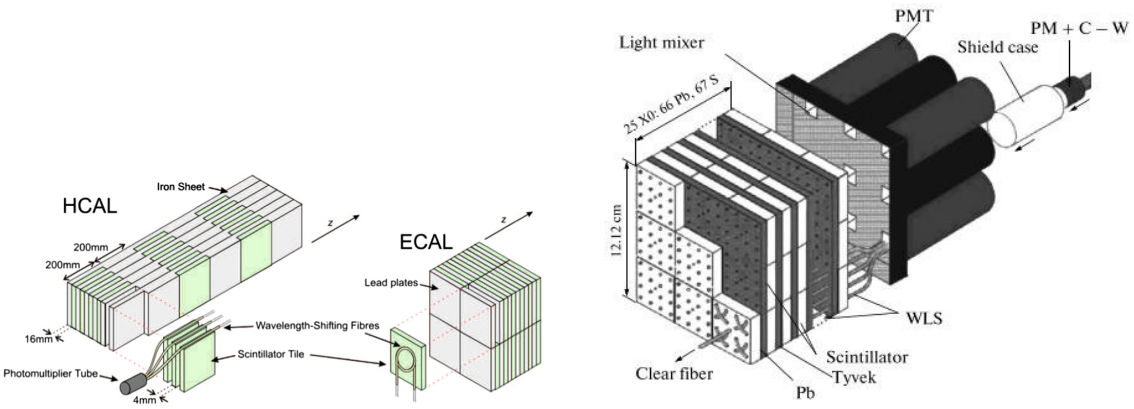


Figure 4.7: Calorimeter System

4.4.3 Muon System

The LHCb muon system is crucial for identifying muons, key decay products of b-hadrons essential for flavor tagging. Located downstream of the calorimeters, it comprises five stations (M1-M5), each divided into four regions (R1-R4) based on distance from the beam axis. This system strategically employs a combination of technologies to optimize performance and cost-effectiveness. In the innermost region (R1) of the first station (M1), where particle flux is highest, Gas Electron Multipliers (GEMs) are utilized. GEMs, consisting of thin, perforated insulating foils coated with conductive material, offer high rate capability, excellent spatial resolution, and radiation hardness, crucial for handling the intense particle environment. Moving outward, Multi-Wire Proportional Chambers (MWPCs) and Drift Tubes (DTs) are employed. MWPCs, with their planes of anode wires between cathode planes [17] [11], provide large area coverage and good time resolution, while DTs, gas-filled tubes with central anode wires, offer robust and cost-effective large-area coverage with good spatial resolution. Muons, due to their penetrating nature, traverse the preceding detectors and leave distinct signals in these muon chambers. By combining signals across the stations, the muon's trajectory is reconstructed. This information is also used in the trigger system to select muon-containing events, making the muon system essential for b-physics studies, CP violation measurements, and searches for new physics.

4.4.4 Flavour Tagging

Many LHCb measurements require the knowledge of the initial flavour (b or $\bar{b}$) of the reconstructed $B^0_{d,s}$ mesons, such as $B^0 - \bar{B^0}$ [18] oscillations and time-dependent CP asymmetries. The process of flavour identification is known as flavour tagging. LHCb utilizes several algorithms that exploit correlations between the B meson's flavor and the properties of other particles produced in the same collision. These algorithms can be broadly divided into two categories:

- **Same-Side (SS) Tagging:** In the hadronization process, other particles are often produced nearby the B meson. Same-side tagging exploits the fact that the electric charge of these nearby particles is correlated with the flavor of the produced B meson. The b quark "picks up" a light quark (or antiquark) from the quark-

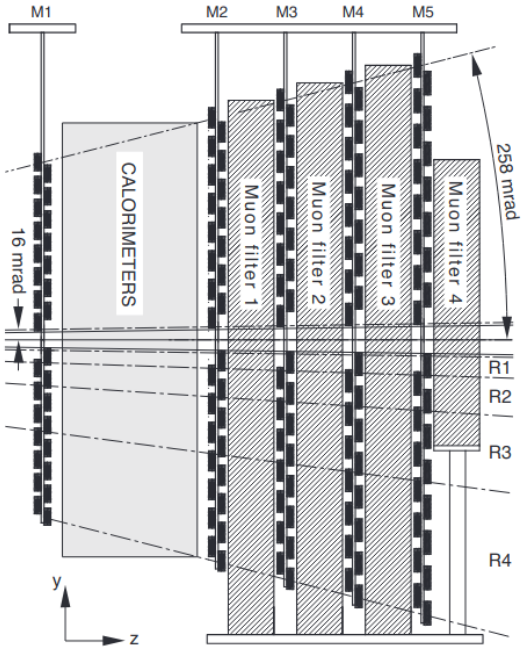


Figure 4.8: Side view of the muon system

gluon vacuum to form a B meson. This process is called fragmentation [13]. In this fragmentation, other particles, mostly pions (π) or kaons (K), are produced in the vicinity of the B meson. If a positive pion (π^+) is produced near a B meson, it suggests that the B meson was a B^0 (b quark + anti-d quark). If a negative pion (π^-) is produced nearby, it suggests the B meson was a B^0 (anti-b quark + d quark). Specifically, when a B_s^0 meson is produced, it's more likely to be accompanied by a K^-, while a B_s^0 meson is more likely to be accompanied by a K^+. Let's say a b quark is produced and it fragments into a B_s^0 meson (b s). This B_s^0 has a strangeness of -1. To conserve strangeness, there needs to be a particle with a strangeness of +1 produced alongside it. A K^- meson (s u) has a strangeness of +1. Therefore, it's more likely to find a K^- produced alongside a B_s^0 meson to balance the strangeness. Similarly, if an anti-b quark is produced and it fragments into a B_s^0 meson (b s), which has a strangeness of +1, it's more likely to be accompanied by a K^+ meson (s d), which has a strangeness of -1, to conserve strangeness.

- **Opposite-Side (OS) Tagging**: Unlike same-side tagging, which looks at particles produced in the same fragmentation process as the B meson, opposite-side tagging

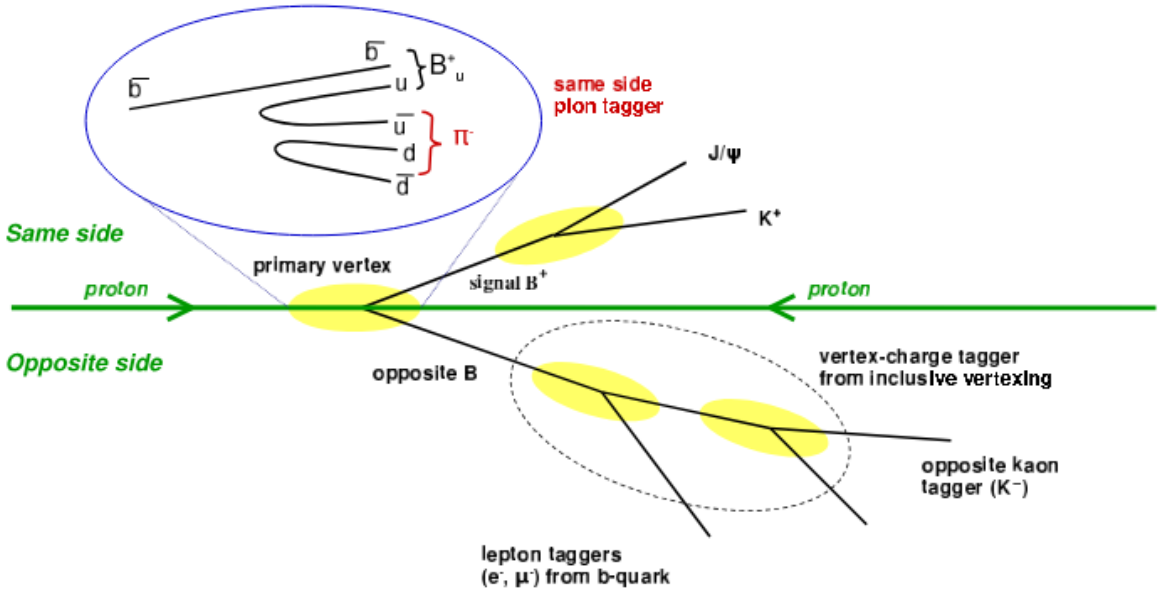


Figure 4.9: Schematic view of the different sources of information available to tag the initial flavour of a signal B candidate

examines the decay products of the other b hadron produced in the collision. If one b hadron is a B^0 (containing an anti-b quark) [13], the other must contain a b quark (e.g., a B^0, B_s^0, or b baryon). The Opposite-Side Muon/Electron is method that identifies muons (μ) or electrons (e) produced in semileptonic decays of the other b hadron. The electric charge of the lepton (μ^+ or e^+ vs mu^- or e^-) is directly correlated with the flavor of the b quark in the decaying hadron. This is because b quarks decay via the weak interaction, typically into a c quark and a W^- boson, which subsequently decays into a μ^- and an antineutrino. Conversely, an anti-b quark decays into an anti-c quark and a W^+ boson, which can then decay into a μ^+ and a neutrino. Therefore, detecting a μ^+ suggests the presence of an anti-b quark in the other b hadron, implying the B meson of interest contained a b quark, while detecting a μ^- suggests the presence of a b quark in the other b hadron, implying the B meson of interest contained an anti-b quark.

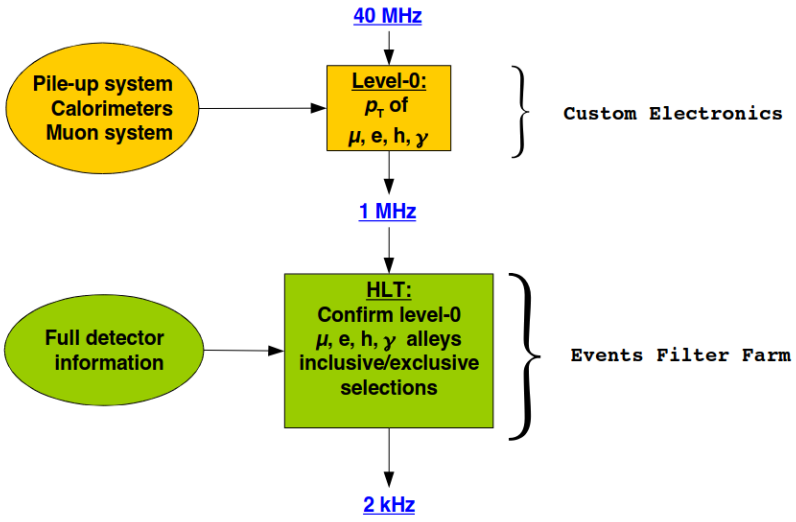


Figure 4.10: Scheme of the LHCb Trigger

4.5 Trigger

The LHCb trigger system is a vital component of the experiment, acting as a highly selective filter to manage the immense data flow from the LHC's proton-proton collisions. With collisions occurring at a frequency of 40 MHz (40 million times per second), it's impossible to store the data from every interaction. The trigger system's primary purpose is to identify and retain only those events that are likely to contain the rare decays of particles containing b quarks, the central focus of LHCb's research. A significant change for Run 3 of the LHC is the removal of the hardware-based Level-0 trigger [17] [11]. Previously, this hardware trigger made extremely rapid decisions based on coarse detector information. Now, LHCb employs a full event readout at the 40 MHz collision rate, meaning data from every collision is initially recorded. This data then passes through a sophisticated software-based High-Level Trigger (HLT) system. The HLT operates in multiple stages, running on a large computing farm. The first stage, HLT1, performs a partial event reconstruction, using information from various detectors to identify promising event candidates.

Critically, HLT1 now runs on GPUs, significantly accelerating processing and enabling more complex algorithms. Subsequently, HLT2 performs a more detailed event reconstruction, applying stricter selection criteria to further reduce the data rate to a manageable level for permanent storage and offline analysis. The trigger system is de-

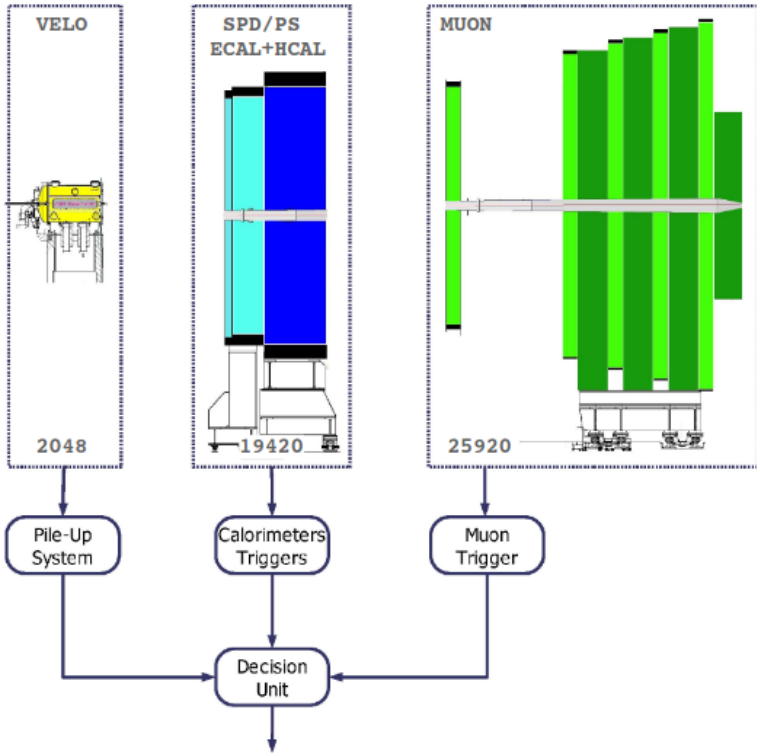


Figure 4.11: Forty million times a second, the Level-0 trigger swiftly processes data from thousands of detector channels: 2048 from pile-up, over 19,000 from calorimeters, and nearly 26,000 from the muon system, to quickly identify potentially interesting collision events.

signed to identify key signatures indicative of b-hadron decays, including particles with high transverse momentum (pT), which are often produced in these decays; displaced vertices, resulting from the short but measurable flight distance of b-hadrons before they decay; and the presence of muons, which are common decay products. The trigger also looks for combinations of these signatures to enhance its efficiency and minimize the selection of background events. This transition to a fully software-based trigger offers several key advantages. It significantly increases the efficiency of selecting relevant events, especially those involving fully hadronic decays, where all final-state particles are hadrons. The software-based approach provides greater flexibility, allowing for more complex and adaptable selection algorithms that can be refined based on new physics insights. Furthermore, this system facilitates real-time analysis, enabling rapid processing and analysis of data, providing immediate feedback on detector performance and potentially accelerating the pace of physics discoveries.

Chapter 5

LHCb Simulation Software

5.1 Gauss

The LHCb experiment uses **Gauss**, its simulation framework built on Gaudi. Gauss handles everything from creating events to modeling how particles move through detectors. This simulation helps with detector design, background estimates, and efficiency studies. Gauss starts by generating events using different tools. PYTHIA simulates general processes, while EvtGen focuses on heavy particle decays. After generating events, Gauss manages particle decays using files that contain information about how particles break down. The core detector simulation runs on GEANT4, which models how particles travel through the LHCb detector. It simulates energy loss, scattering [10] [8], and the creation of new particles. This creates realistic detector signals that match what the real detector would produce. Gauss follows a simple workflow: generate initial particles, simulate them moving through the detector, and save the results in a format that works with the same software used for real data. To keep up with new demands, they've developed an improved version called Gaussino that's faster and more efficient. This ensures Gauss can handle future LHCb experiments. Basically, Gauss is a key tool for understanding particle physics at LHCb - not just a simulation program.

5.2 Gaussino

Gaussino is both a **library** and a **standalone** application created from Gauss. It's a big improvement in LHCb's simulation abilities, designed to handle the challenges of

Run 3 and future LHC data collection. They developed it because they needed better performance, more flexibility, and the ability to use multiple processor cores at once. The main reason for creating Gaussino was the expected increase in collision data during Run 3. More collisions mean more complex events and much more data to process. The old system worked but was too rigid and couldn't effectively use modern multi-core processors. Gaussino improves things in several ways. It separates LHCb-specific parts from the general simulation framework, making the code cleaner and potentially useful for other experiments. The code has been updated using modern C++ practices. It works better with GEANT4 (the standard toolkit for simulating particles) and fully uses multi-threading to run simulations much faster. It also allows for faster simulation methods when detailed simulations aren't needed, and it's designed to work with machine learning techniques. In the current setup, Gauss uses Gaussino as its core engine - Gauss handles LHCb-specific settings while Gaussino handles the basic simulation tasks. The impact on LHCb is significant. Better performance means they can produce larger simulated datasets, crucial for precise physics analysis. The improved flexibility makes it easier to develop new detector designs. And the ability to use fast simulation and machine learning opens up new research possibilities that were previously too computationally demanding. Essentially, Gaussino represents a complete rethinking of LHCb's simulation capabilities, keeping the experiment at the forefront of particle physics research in the high-luminosity LHC era.

Chapter 6

Setup and Detector Geometry

6.1 ParticleGun

The LHCb experiment uses this tool called ParticleGun in their Gauss simulation framework. Unlike big event generators like PYTHIA that simulate entire collision events, ParticleGun is more specialized - it just generates individual particles or simple particle beams that you can customize. What makes ParticleGun useful is how much control it gives you. You can specify exactly what type of particle you want, set its momentum or energy (either as fixed values, ranges, or distributions), control its direction (fixed direction, within a cone, or spreading in all directions), and choose where it starts from. This level of control is super helpful for several detector-related tasks. Scientists mainly use ParticleGun for calibrating detectors, where they need particles with known properties to properly calibrate different detector components. It's also great for alignment studies - researchers can see how misalignments affect particle paths. Beyond that, ParticleGun helps with evaluating detector performance, studying backgrounds, and simulating test beam conditions. The big advantage of ParticleGun is that it's much simpler and computationally lighter than full event generators, making it perfect for focused detector studies at LHCb when you don't need to simulate entire collision events.

6.2 Fast Calorimeter Simulation

Fast calorimeter simulation is a crucial technique in high-energy physics, offering a computationally efficient alternative to full detector simulations like GEANT4. While full

simulations meticulously model every particle interaction within the calorimeter, fast simulations employ parameterizations and simplified models to approximate the calorimeter's response. [6] This allows for the rapid generation of large simulated datasets, essential for tasks like detector optimization, trigger development, and large-scale background studies. Fast simulations typically parameterize the shower development within the calorimeter based on experimental data or simplified shower models. These parameterizations describe key shower properties, such as energy deposition profiles, longitudinal and transverse shower shapes, and energy resolution. Instead of tracking every particle individually, fast simulations use these parameterizations to directly estimate the energy deposited in the calorimeter cells. This drastically reduces the computational cost compared to full simulations, enabling the simulation of significantly more events in a given timeframe. While sacrificing some level of detail, fast simulations provide valuable insights and are often sufficient for many analysis tasks, especially in early stages of detector design and physics studies.

6.2.1 Why Calorimeter?

Fast simulation is particularly important for calorimeters due to the complexity of simulating hadronic showers, which involve numerous particles and interactions. Detailed simulations of these showers are computationally expensive, and the inherent fluctuations necessitate simulating a large number of events. Fast simulation makes this feasible. Furthermore, calorimeters are vital for triggering on interesting events and identifying backgrounds. Fast simulation is essential for developing and optimizing trigger algorithms and generating the large background samples needed for accurate physics analyses. While fast simulation can be applied to other detector components, the gains in computational efficiency are most significant for calorimeters, making it a crucial tool for high-energy physics experiments.

6.3 CaloChallenge

The CaloChallenge stands as a significant community-driven initiative dedicated to pushing the boundaries of fast calorimeter simulation within high-energy physics. Recognizing the computational limitations of full detector simulations, such as those performed

with GEANT4, the CaloChallenge provides a platform for researchers to develop, test, and compare computationally efficient alternatives. While full simulations meticulously track every particle interaction within the calorimeter, fast simulations employ parameterizations, simplified models, and increasingly, generative machine learning models, to approximate the calorimeter's response. This trade-off between accuracy and computational speed is crucial for various tasks, including detector optimization, trigger development, and large-scale background studies, where simulating vast numbers of events is paramount. The core of the CaloChallenge revolves around a shared, meticulously generated dataset of calorimeter showers produced using a full detector simulation. This common dataset serves as the benchmark against which different fast simulation techniques are evaluated, ensuring a fair and direct comparison. Participants develop their own fast simulation methods, which are then used to generate simulated calorimeter showers corresponding to the events in the common dataset. [5]

The performance of these fast simulation methods is rigorously assessed using a range of well-defined evaluation metrics. These metrics encompass various aspects of the simulated showers, including comparisons of one-dimensional and multi-dimensional distributions of shower properties, such as energy deposition profiles, longitudinal and transverse shower shapes, and energy resolution. Statistical distances, like those calculated using the Kolmogorov-Smirnov test, are employed to quantify the agreement between the fast and full simulation outputs. Furthermore, the effectiveness of classifiers trained to distinguish between fast and full simulation samples is used as a powerful discriminator. A significant focus of recent CaloChallenges has been the exploration of generative machine learning models for fast simulation. These models, such as Generative Adversarial Networks (GANs) and Variational Autoencoders (VAEs), learn the underlying probability distribution of calorimeter showers from the training data generated by full simulations. Once trained, these models can rapidly generate new, realistic calorimeter showers, offering a promising avenue for achieving both accuracy and speed in fast simulation.

6.3.1 Geometry

The CaloChallenge employs simplified detector geometries to provide a standardized benchmark for fast calorimeter simulation methods. Typically, a cylindrical geometry is used, mimicking the approximate symmetry of many real-world calorimeters. Particles

are incident along the cylinder's axis (z-axis). [5] The calorimeter is segmented both longitudinally and transversely. Longitudinal segmentation divides the calorimeter into layers along the z-axis, representing different depths. Transverse segmentation further divides each layer into radial bins (distance from the beam axis) and sometimes azimuthal bins (angle around the beam axis). Specific parameters like the number of layers, radial and azimuthal bins, layer thickness and material, and inner/outer radii are defined in configuration files accompanying the datasets. While simplified, these geometries capture key features of shower development, including longitudinal shower profiles, transverse spread, and energy containment, allowing for focused comparison of fast simulation techniques without the complexities of full detector descriptions.

6.4 Setup

In this work, we have used **ParticleGun** to generate and send gammas towards somewhat in the middle of the ECAL. We want to see how the detector responds to these hits in case of both AdePT with GEANT4 vs GEANT4 alone and compare the results. For our purpose, we have generated 1000 events, with 1 gamma per event, using a particular detector geometry, **CaloChallenge** [4].

Chapter 7

Monitoring Plots of GEANT4 + AdePT vs GEANT4

Simulation monitoring plots are crucial for ensuring the quality and reliability of high-energy physics simulations. These plots provide visual checks on the correctness of the simulation setup, allowing for early detection of issues like incorrect geometry or physics models. They aid in understanding detector response by visualizing particle interactions and energy deposition, and they are essential for evaluating detector performance. Monitoring plots also track simulation progress, helping determine convergence and manage resources. Furthermore, they facilitate the identification of unexpected distributions or outliers, which can point to potential problems. Finally, these plots serve as valuable tools for communication and collaboration, enabling researchers to easily share and document simulation results. The following are the monitoring plots that evaluates the performance of GEANT4 with AdePT and GEANT4 stand-alone. A description of each plot is provided as its caption.

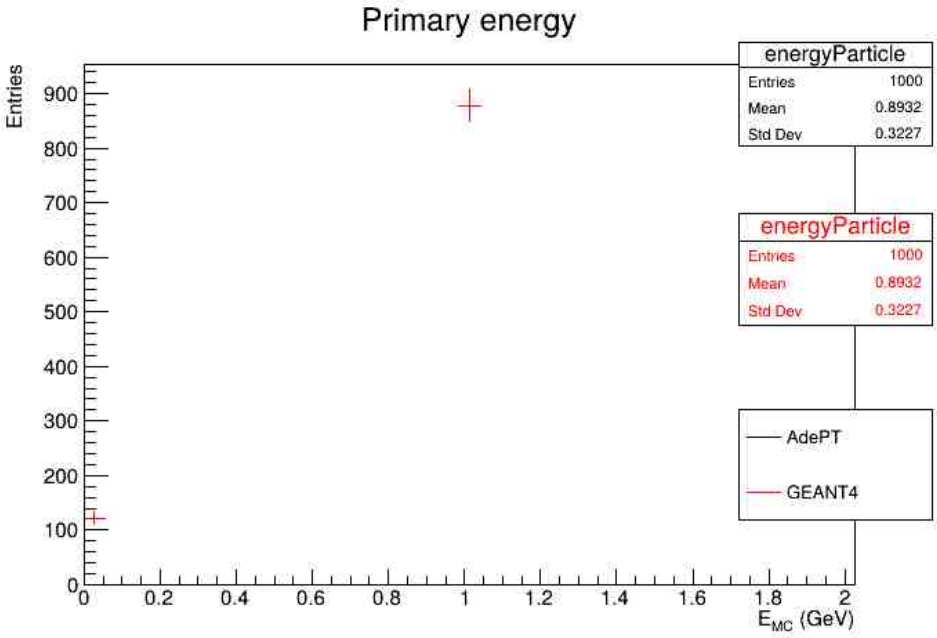


Figure 7.1: Shows the energy distribution of the primary particles that are generated by the simulation. It helps one verify that one has correctly defined the energy spectrum of the primary particle source in the simulation.

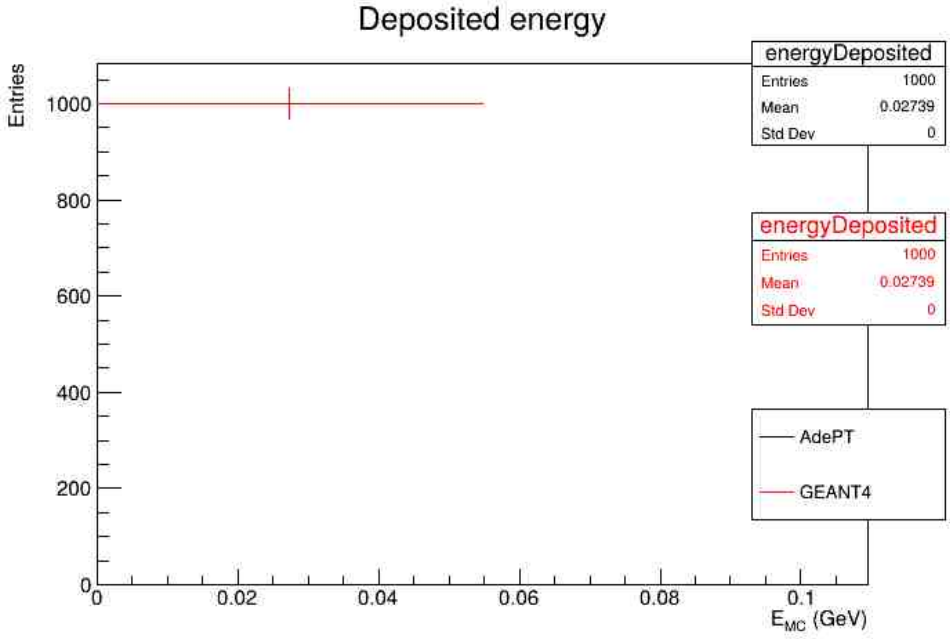


Figure 7.2: Visualizes the spatial distribution and magnitude of energy lost by particles as they interact with ECAL. These plots, often 2D or 3D histograms, are crucial for understanding detector response, validating simulations against experimental data, calibrating detectors, and performing physics analyses by revealing energy deposition patterns and shower profiles.

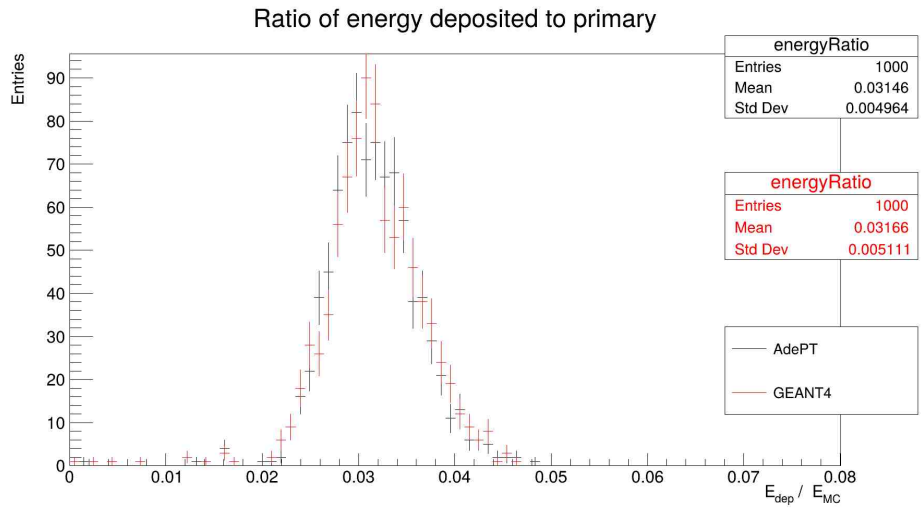


Figure 7.3: Helps one understand how well one's detector is. By comparing the distribution of this ratio from your simulation to experimental data, one can assess how well your simulation is modeling the detector's response. If the simulated ratio distribution doesn't match the data, it suggests there might be issues with your simulation geometry, material properties, physics models, or calibration.

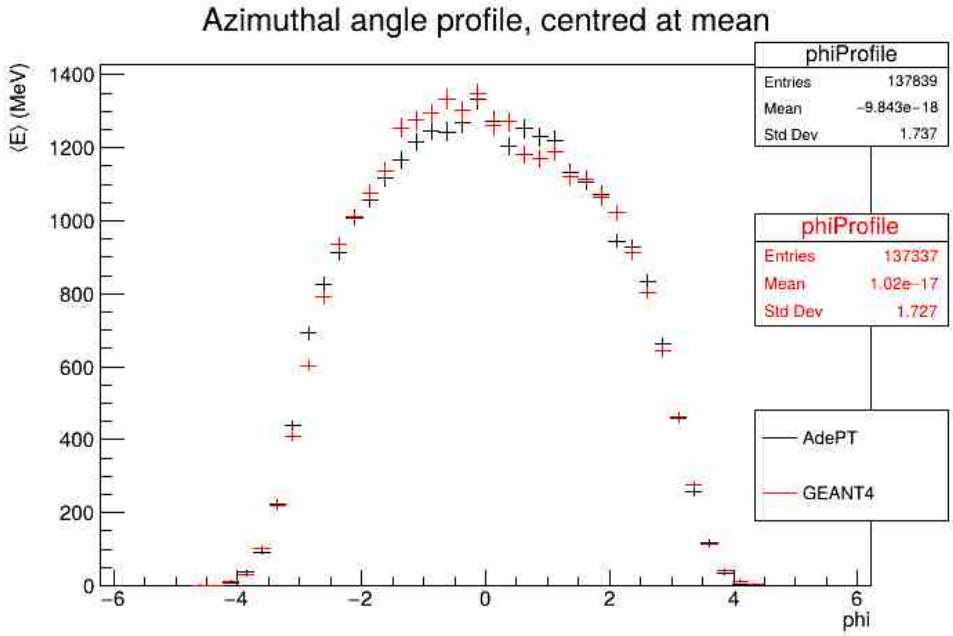


Figure 7.4: Variations in the RMS energy as a function of *phi*, it could indicate that some cells in your ECAL are more susceptible to fluctuations in energy deposition than others.

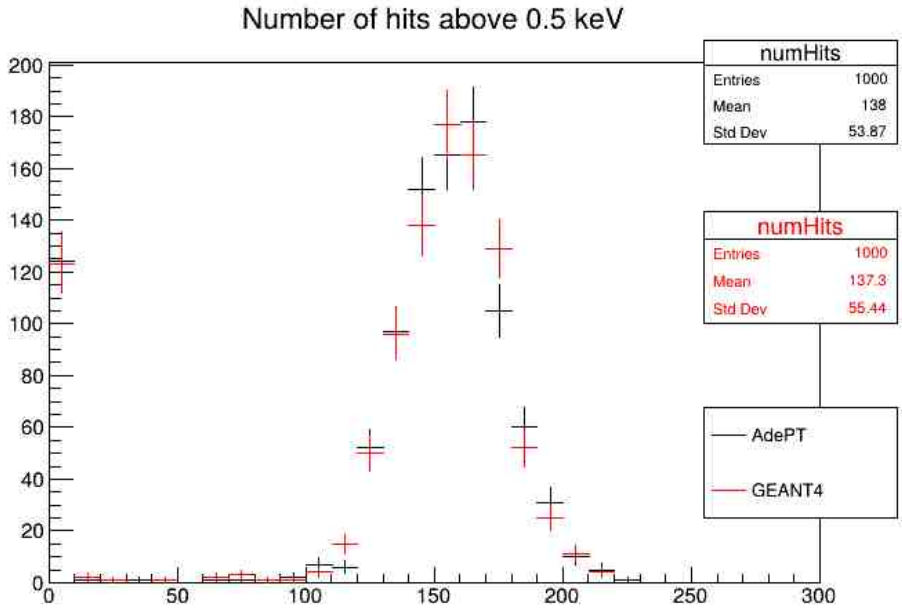


Figure 7.5: 0.5 keV might be the lowest energy the ECAL in the CaloChallenge setup can reliably measure.

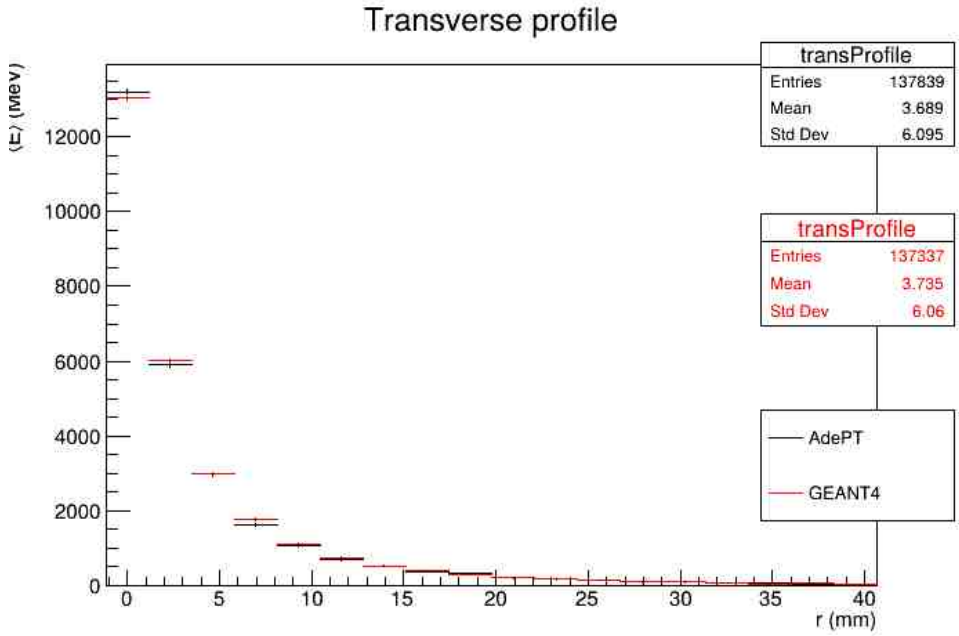


Figure 7.6: In the context of a forward spectrometer, transverse profile shows energy deposition at the detector plane, where **r** is the distance from the beam axis at the detector location, related (but not directly equal) to the production angle of the particles. This plot is important for understanding the detector acceptance, optimizing its design, and performing physics analyses in the forward region.

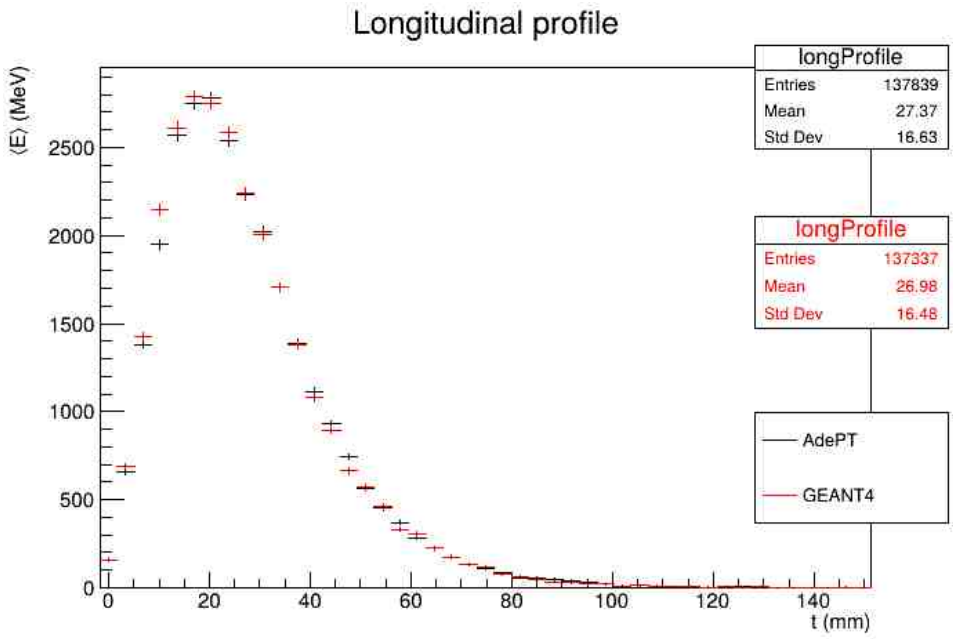


Figure 7.7: A longitudinal profile of energy deposition in a calorimeter shows how the energy deposited by an incoming particle shower develops as a function of depth. This helps understand how the calorimeter measures energy.

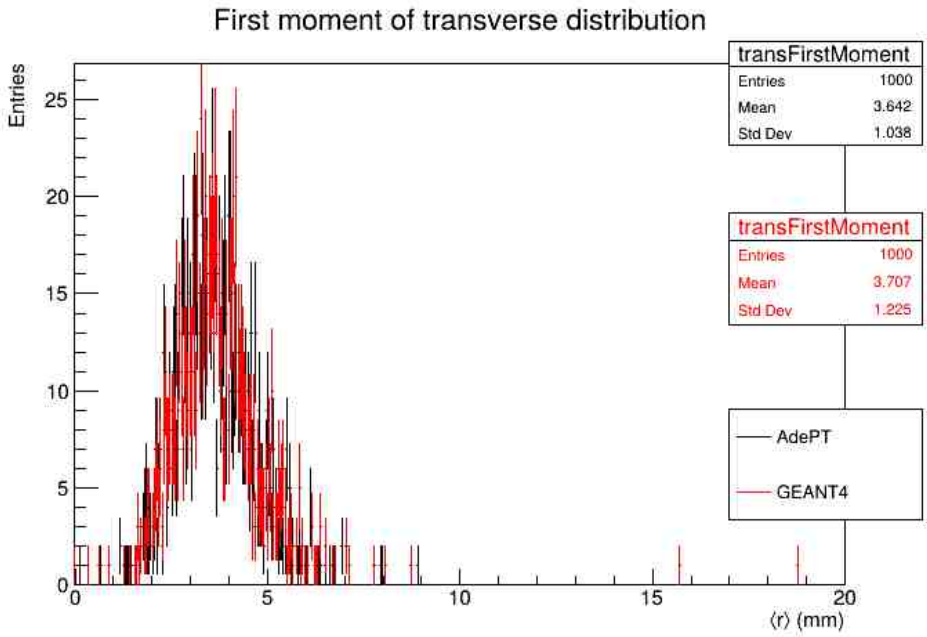


Figure 7.8: The first moment pf a transverse profile provides information about the average or mean position of the distribution along the transverse direction. It essentially tells you where the "center of mass" of the distribution is located.

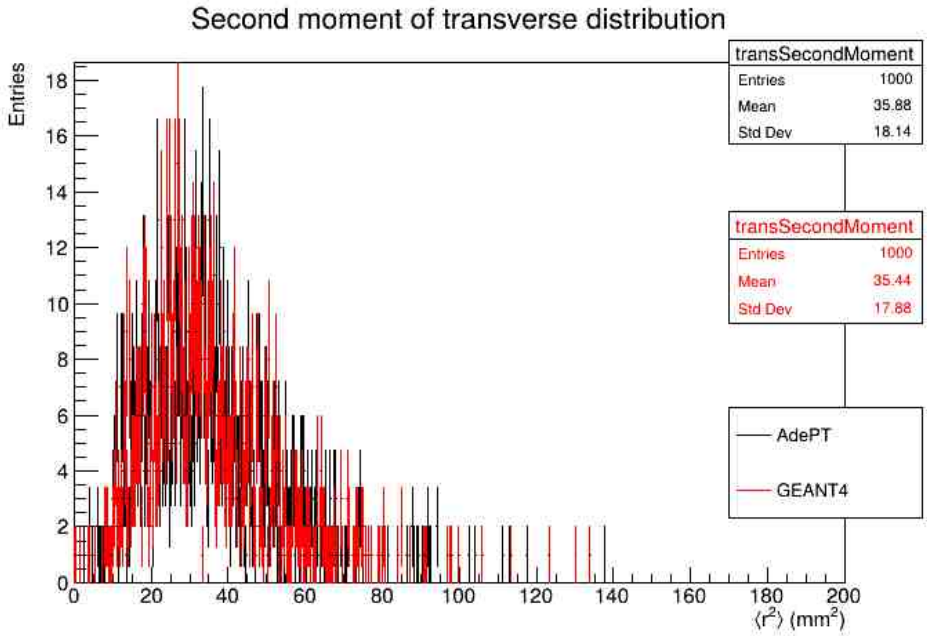


Figure 7.9: The second moment of a transverse distribution plot is a valuable tool for understanding the spread or width of the distribution, which is crucial in various applications, from characterizing beam size to determining detector resolution.

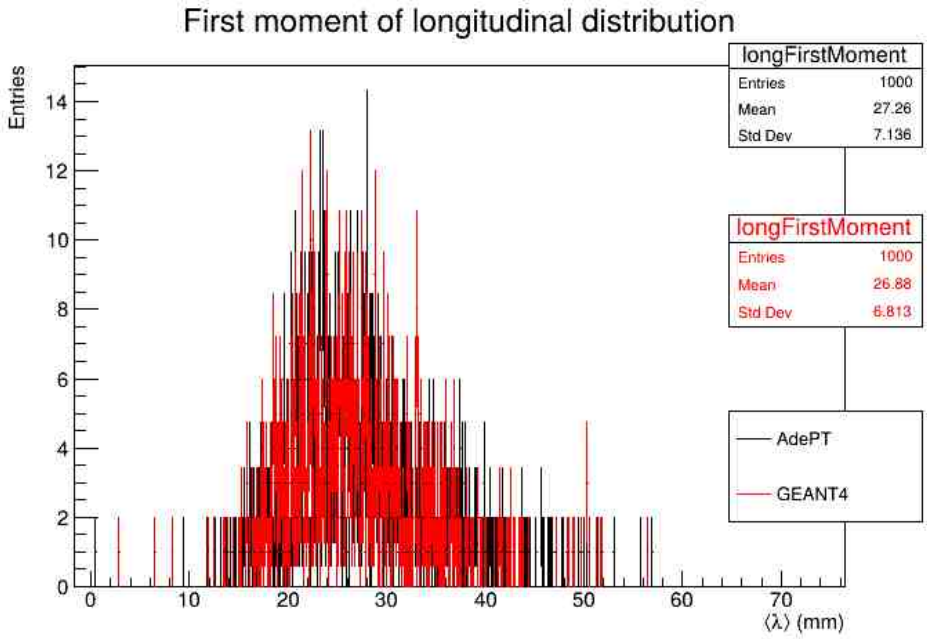


Figure 7.10: The first moment of a longitudinal profile tells you the average depth or position where the quantity is concentrated. It's the point along the detector's length where the distribution would be perfectly balanced.

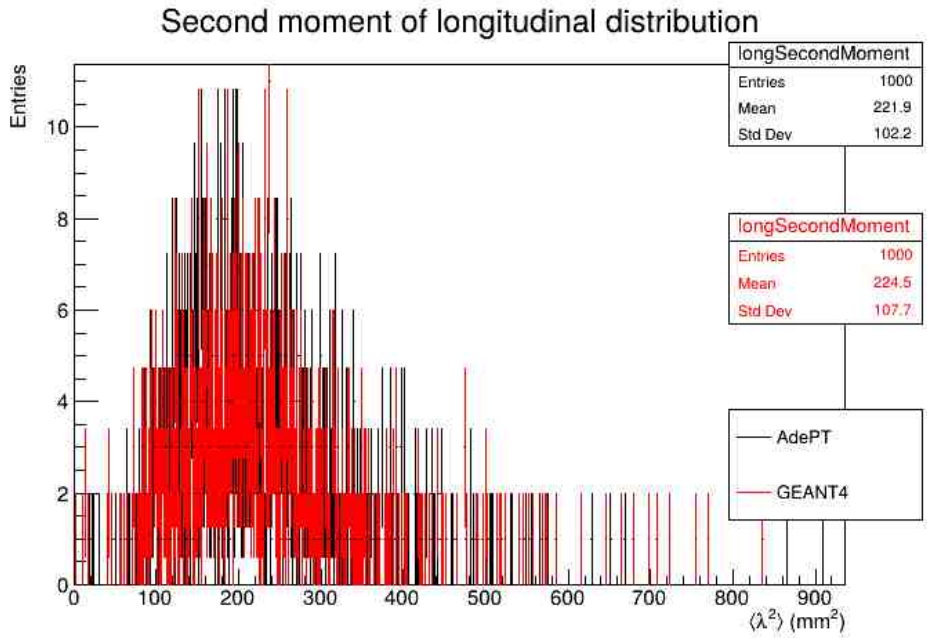


Figure 7.11: In calorimeters, the second moment of the longitudinal energy deposition profile gives you information about the longitudinal development of the particle shower. A wider distribution indicates a shower that extends over a larger range of depths.

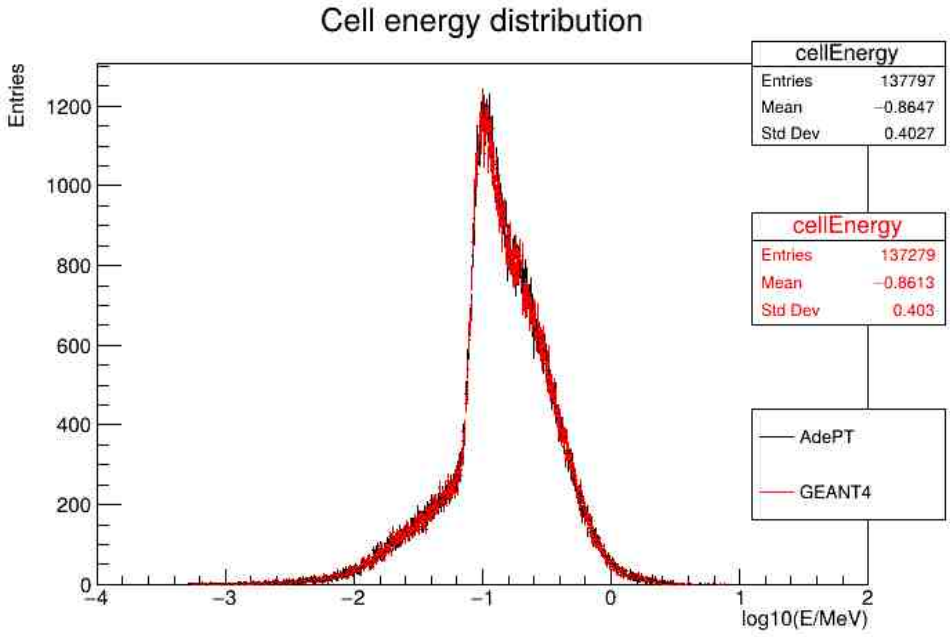


Figure 7.12: Distribution of energy deposited within the individual 6016 cells of the ECAL.

Key Observations

1. Refer to Figure 7.13.

2. AdePT, being GPU-accelerated, is expected to give a faster simulation than GEANT4 or Gaussino stand-alone, but that was not the case in this particular part of the project. But, a different setup, where this time we sent 1000 gammas per event, has caused AdePT (`Throughput[1/s]:2.762e+00`) to run over 7 times faster than GEANT4 or Gaussino stand-alone (`Throughput[1/s]:3.550e-01`).

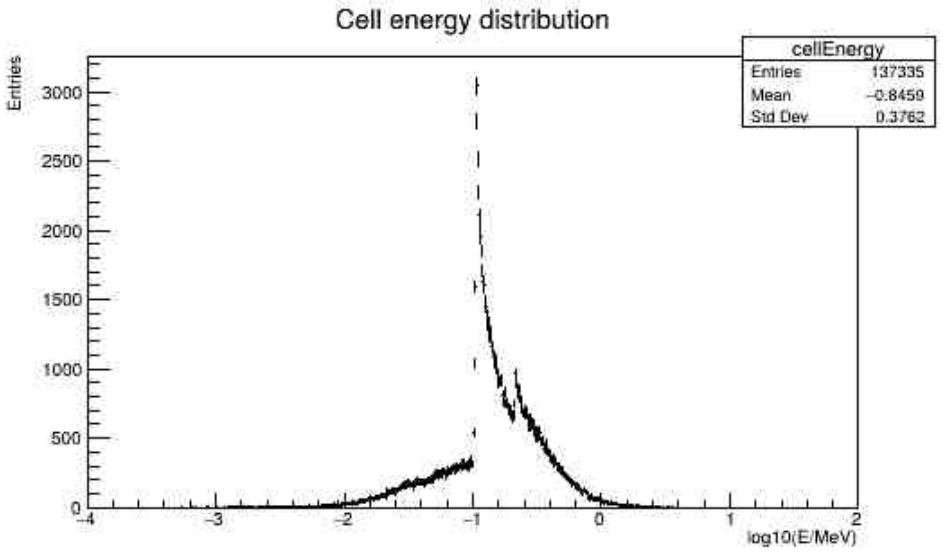


Figure 7.13: Initial cell energy distribution. [7] The discrepancy between 39 and 40 is because, initially, energy loss fluctuations were switched off for AdePT, although they were implemented in the physics library **G4HepEm**.

Chapter 8

Conclusion

For the part of the project where we used CaloChallenge detector geometry, AdePT and GEANT4 surely have really good agreement, as can be inferred from the histograms, but the simulation has taken much longer time for AdePT rather than GEANT4. Sending 1000 gammas instead of 1 gamma per event caused AdePT to run faster than GEANT4 and this demonstrates clearly that in order to benefit from GPU simulation, one needs to have a lot of particles per event sent to it. So, maybe depending on the events one may need to decide whether one wants to use the GPU or not.The main current goal of AdePT is to prove that we can run general HEP simulation on GPUs and that we are getting correct physics results, which, in this project, we have successfully shown by producing several good plots. This study shows that GPU-based simulation can be cannot automatically make all the simulations faster. Due to the specificity of the GPUs there is the condition of having many particles to be simulated at once which cannot be always satisfied. AdePT is continuing the R&D to improve the workflows and to allow an efficient use of the GPUs in as many cases as possible. This particular work is going to be one of the Gaussino examples that will be released and available for everyone to try out and the results in particular have been presented in the **Conference on Computing in High Energy and Nuclear Physics**, on 21/10/2024 in CERN [3].

Appendix A

Estimating the Volume of n-sphere using Monte Carlo

To understand the basic principle of what a Monte Carlo method essentially does, finding the volume of an n-sphere is a good example. An n-sphere is basically a sphere with an n-dimensional surface. For example, the surface of a 3-sphere (our regular sphere) is 2-dimensional. The following approach or algorithm can be implemented in any programming language.

Steps:

1. **Generate random points inside a hypercube:** In an n-dimensional space, we generate random points in the hypercube $[0, R]^n$. A hypercube is a generalization of a cube to any number of dimensions.These points are drawn from a uniform distribution. For example, if $n = 2$, we are generating points (p_1, p_2) where both p_1 and p_2 are in the range $[0, R]$. If $n = 3$, we generate points (p_1, p_2, p_3), where each coordinate is between 0 and R.

2. **Check if the points are inside the n-sphere:** We check if each point lies inside the n-sphere with radius R. A point $p = (p_1, p_2, \ldots, p_n)$ is inside the n-sphere if the following condition holds:

$$\sum_{i=1}^{i=n} p_n^2 \leq R^2$$

3. **Estimate the volume:** The ratio of points inside the n-sphere to the total points generated gives us an estimate of the ratio of the volume of the n-sphere to the volume of the n-dimensional cube. The volume of the cube in n-dimensions is R^n,

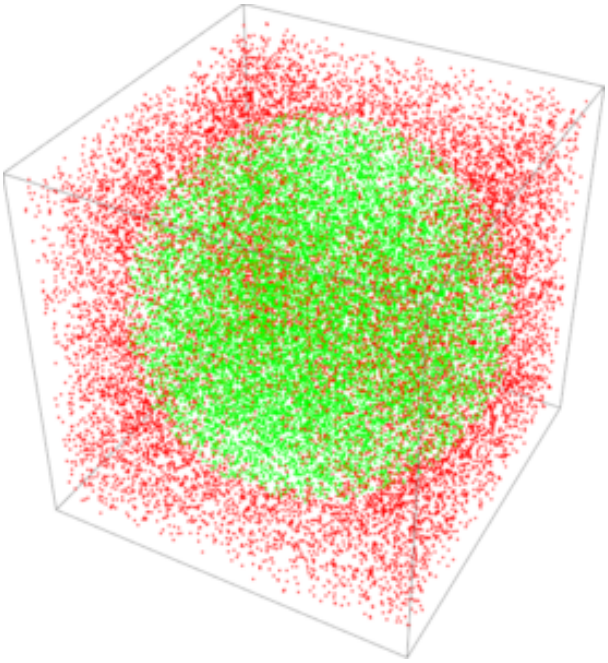


Figure 8.1: Random sampling points in n-dimensional spheres to find the volume of n-sphere.

so:

$$V_n = \frac{\text{Number of points inside the n-sphere}}{\text{Total number of points generated}} \times R^n$$

The formula for the volume of an n-sphere is

$$V_n(R) = \frac{\pi^{\frac{n}{2}}}{\Gamma(\frac{n}{2}+1)} R^n$$

One can easily verify that the result from the Monte Carlo implementation matches approximately with the values obtained using this formula.

Appendix B

Monte Carlo Simulation of Radioactive Decay

Imagine you have a sample of radioactive atoms. Each atom has a certain probability of decaying within a given time interval. You want to know how many atoms will remain undecayed after a certain amount of time. [16]

The Monte Carlo Approach:

1. **Define the model:** You know the decay constant λ of the radioactive isotope, which is related to the probability of decay per unit time.

2. **Introduce Randomness:** The decay of each individual atom is a random event. We can model this using a random number generator.

3. **Generate Random Samples:** For each atom in your sample, generate a random number between 0 and 1.

4. **Run Simulations:** For each atom:

    - If the random number is less than $e^{-\lambda t}$ (where t is the time elapsed), the atom has decayed.
    - If the random number is greater than or equal to $e^{-\lambda t}$, the atom remains undecayed.

5. **Analyze Results:**

    - Count the number of atoms that remain undecayed after simulating the decay of all atoms in your sample.

- Repeat steps 3-5 many times (e.g., thousands of times) to get a distribution of possible outcomes.

Table 1 shows a sample and simulation results from [citation]. The corresponding plot is shown in Figure 41.

t	N(t) (Using Random Numbers Method)	$N(t) = N_0 e^{-\lambda t}$
0	200	200
1	160	164
2	126	134
3	105	110
4	81	90
5	71	74
6	59	60
7	51	49
8	44	40
9	35	33
10	30	27
11	25	22
12	21	18
13	19	15
14	18	12
15	13	10

Table 8.1: Starting sample of $N_0 = 200$ and decay constant $\lambda = 0.2$

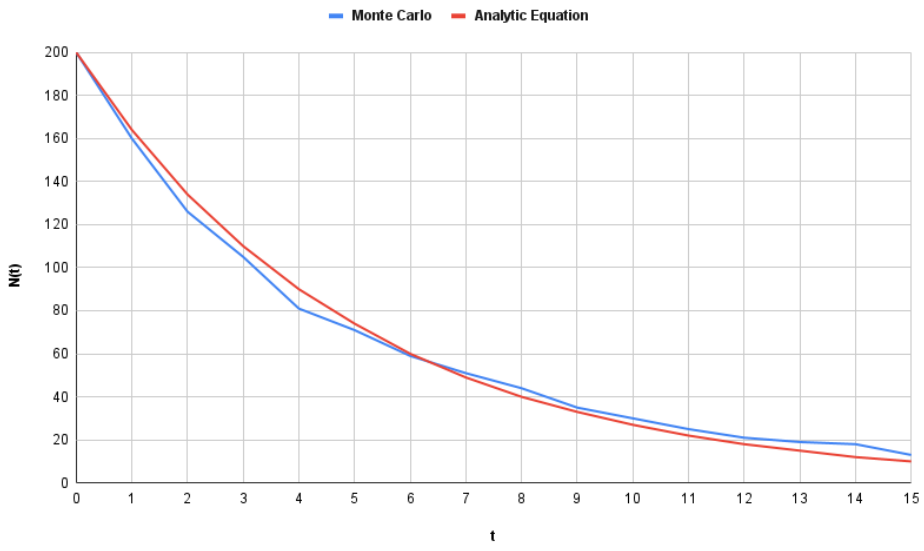


Figure 8.2: Monte Carlo vs Analytic Equation for $N_0 = 200$ and $\lambda = 0.2$

Appendix C

Derivation of Pseudorapidity

Prior knowledge of Special Relativity is required to understand the origin of Lorentz transformation, rapidity, the γ factor and mass-energy relation.

Recall from Special Relativity, [22] a boost along the z - axis with speed v is equivalent to a hyberbolic rotation through an amount α, known as the rapidity, given by $\tanh \alpha = \beta$, where $\beta = v/c$,

$$\begin{aligned} \tanh \alpha &= \beta \\ \beta &= \frac{e^{2\alpha} - 1}{e^{2\alpha} + 1} \\ \alpha &= \frac{1}{2} \ln \frac{1+\beta}{1-\beta} \end{aligned}$$

Since,

$$\begin{aligned} \frac{p}{E} &= \frac{\beta}{c} \\ \beta &= \frac{pc}{E} \end{aligned}$$

and taking $c = 1$, we have

$$\begin{aligned} \alpha &= \frac{1}{2} \ln \frac{1+\beta}{1-\beta} \\ \alpha &= \frac{1}{2} \ln \frac{E+p}{E-p} \end{aligned}$$

Performing Lorentz boost to this equation,

$$\begin{aligned}\alpha' &= \frac{1}{2}\ln\frac{\gamma E - \beta\gamma p_z + \gamma p_z - \beta\gamma E}{\gamma E - \beta\gamma p_z - \gamma p_z + \beta\gamma E} \\ &= \frac{1}{2}\ln\frac{E + p_z}{E - p_z} + \ln\sqrt{\frac{1-\beta}{1+\beta}} \\ \alpha' - \alpha &= \tanh^{-1}\beta\end{aligned}$$

This is the beauty of rapidity and the reason why it is used in high energy physics. The difference between the rapidities of two particles under a Lorentz boost remains constant whereas all other dynamical variables change. The only problem with rapidity is that it can be hard to easure for highly relativistic particles, since in reality, it is often difficult to get the total momentum of a particle.

But, knowing that for a highly relativistic particle, p >> m, therefore,

$$\begin{aligned}\alpha &= \frac{1}{2}\ln\frac{p(1+\frac{m^2}{p^2})\frac{1}{2} + p_z}{p(1+\frac{m^2}{p^2})\frac{1}{2} - p_z} \\ &\approx \frac{1}{2}\ln\frac{1+\frac{p_z}{p}}{1-\frac{p_z}{p}}\end{aligned}$$

Now, $\frac{p_z}{p} = \cos\theta$, where θ is the angle made by the particle trajectory with the beam pipe and hence we have

$$1 + \frac{p_z}{p} = 1 + \cos\theta = 2\cos^2\frac{\theta}{2}$$

and

$$1 - \frac{p_z}{p} = 2\sin^2\frac{\theta}{2}$$

Therefore,

$$\alpha \approx \frac{1}{2} \ln \frac{cos^2 \frac{\theta}{2}}{\sin^2 \frac{\theta}{2}}$$
$$\alpha \approx -\ln \tan \frac{\theta}{2}$$

We define this quantity as the pseudo-rapidity,

$$\eta = -\ln \tan \frac{\theta}{2}$$

Bibliography

[1] AdePT, The LHCb Collaboration, *AdePT*, GitHub. Available at: https://github.com/apt-sim/AdePT. (accessed from June 24 - August 16, 2024)

[2] AdePT, The LHCb Collaboration, *Offloading electromagnetic shower transport to GPUs*, 2022. Available at: https://arxiv.org/pdf/2209.15445

[3] AdePT, The LHCb Collaboration, *AdePT - Enabling GPU electromagnetic transport with Geant4*, 2024. Available at: https://indico.cern.ch/event/1338689/contributions/6015934/attachments/2951401/5188875/AdePT%20-%20CHEP%202024.pdf

[4] The LHCb Collaboration, *CaloChallenge*, GitHub. Available at: https://gitlab.cern.ch/Gaussino/Gaussino/-/tree/mimazure-calo-challenge/Sim/CaloChallenge/python/CaloChallenge .(accessed from June 24 - August 16, 2024)

[5] The LHCb Collaboration, *CaloChallenge*, GitHub, 2024. Available at: https://arxiv.org/pdf/2410.21611 .(accessed from June 24 - August 16, 2024)

[6] Ali Hariri, Darya Dyachkova, Sergei Gleyzer, *Graph Generative Models for Fast Detector Simulations in High Energy Physics*, 2021. Available at: https://arxiv.org/abs/2104.01725

[7] CERN, *Energy Loss Fluctuations, Electromagnetic Interaction, GEANT4*. Available at: https://geant4-userdoc.web.cern.ch/UsersGuides/PhysicsReferenceManual/html/electromagnetic/energy_loss/fluctuations.html.

[8] The LHCb Collaboration, *Gauss*, GitHub. Available at: https://lhcb-gauss.docs.cern.ch/master/. (accessed from June 24 - August 16, 2024)

[9] The LHCb Collaboration, *Gaussino*, GitHub. Available at:https://gaussino.docs.cern.ch/master/. (accessed from June 24 - August 16, 2024)

[10] The LHCb Collaboration, *The LHCb simulation software Gauss & its Gaussino core framework*, 2022. Available at: https://cds.cern.ch/record/2838826/files/gloria_corti.pdf

[11] The LHCb Collaboration, *Everything you wanted to know about LHCb. but were afraid to ask.* Avaiable at: https://cds.cern.ch/record/2694176/files/LHCbImplications_v2%2016.10.pdf.

[12] T. Sjöstrand, *Monte Carlo Event Generation. for LHC*, 1991. Available at: http://home.thep.lu.se/~torbjorn/preprints/th6275.pdf

[13] Claire Prouve, Niklas Nolte, and Christoph Hasse, *Fast Inclusive Flavour Tagging at LHCb*, 2024. Available at: https://arxiv.org/pdf/2404.14145

[14] The LHCb Collaboration, *THE LHCb PHYSICS PROGRAMME*, 2001. Available at: https://cds.cern.ch/record/794033/files/Pages_from_C99-03-20.1_409.pdf

[15] N. Tuning, *Lecture Notes on CP Violation*, 2020. Available at: https://www.nikhef.nl/~h71/Lectures/2020/ppII-cpviolation-14022020.pdf

[16] Sahajpreet Singh, *Monte Carlo Simulation of Radioactive Decay*, 2020. Available at: https://www.ijeast.com/papers/86-90,Tesma505,IJEAST.pdf

[17] The LHCb Collaboration, *The LHCb Detector at the LHC*, 2008. Available at: https://cds.cern.ch/record/1129809/files/jinst8_08_s08005.pdf

[18] Miriam Calvo Gomez [LHCb Collaboration], *Flavour Tagging at LHCb*, 2012. Available at: https://indico.cern.ch/event/164272/contributions/1420483/attachments/196553/275851/mcalvo.pdf

[19] W. Pokorski, R. Chytracek, J. McCormick, G. Santin, *GEOMETRY DESCRIPTION MARKUP LANGUAGE AND ITS APPLICATION-SPECIFIC BINDINGS.*

Available at: https://indico.cern.ch/event/408139/contributions/979922/attachments/815913/1118019/GDML_CHEP06.pdf

[20] Claude Itzykson & Jean-Bernard Zuber, *Quantum Field Theory* (1980)

[21] Glenn F. Knoll, *Radiation Detection and Measurement* (4th Edition, 2010)

[22] Graham Shaw, Brian R. Martin, *Particle Physics* (2008)

[23] O. Brüning, H. Burkhardt, S. Myers, The large hadron collider, 2012. Available at: https://indico.cern.ch/event/184080/contributions/1455617/attachments/252027/352392/The-Large-Hadron-Collider_Bruening-Burkhardt-Myers.pdf